DOE-RMOTC-51065

HYDROGEOPHYSICS, INC.: HIGH RESOLUTION RESISTIVITY MONITORING OF A SURFACTANT FLOOD FOR ENHANCED OIL RECOVERY

Final Report for the Period of May 2006 to January 2007

Date Completed: March 2007

By:
James B. Fink, Richard J. Wold, Dale F. Rucker, Marc T. Levitt and John B. Fleming, hydroGEOPHYSICS, Inc.
Lyle A. Johnson, RMOTC

Prepared for the United States Department of Energy
Office of Fossil Energy

Work performed under Rocky Mountain Oilfield Testing Center (RMOTC)
CRADA 2006-070

This document may contain protected CRADA information produced under CRADA no. 2006-070 and is not to be further disclosed for a period of 5 years from the date it was produced except as expressly provided for in the CRADA

DISCLAIMER

This report was prepared as an account of work sponsored by an agency of the United States Government. Neither the United States Government nor any agency thereof, nor any of their employees, nor any of their contractors, subcontractors or their employees, makes any warranty, expressed or implied, or assumes any legal liability or responsibility for the accuracy, completeness, or any third party's use or the results of such use of any information, apparatus, product, or process disclosed, or represents that its use would not infringe privately owned rights. Reference herein to any specific commercial product, process, or service by trade name, trademark, manufacturer, or otherwise does not necessarily constitute or imply its endorsement, recommendation, or favoring by the United States Government or any agency thereof or its contractors or subcontractors. The views and opinions of authors expressed herein do not necessarily state or reflect those of the United States Government or any agency thereof.

ABSTRACT

hydroGEOPHYSICS, Inc. (HGI) and the Rocky Mountain Oilfield Testing Center (RMOTC) jointly conducted a test of HGI's patented High Resolution Resistivity (HRR) subsurface fluid monitoring technology to demonstrate the effectiveness of a non-intrusive measurement method to monitor fluid movement during a series of formation water and surfactant floods designed for enhanced oil recovery (EOR). The project was located at the Naval Petroleum Reserve No. 3 (NPR-3), and the floods occurred in the Shannon Sandstone Member of the Upper Cretaceous Steele Formation.

The monitoring technology, HRR, is based on a time series analysis of a direct-current electrical geophysical method. The method relies on contrasts in electrical properties between the host formation and that of the injected fluid, and uses existing metallic infrastructure such as the casing of oilfield wells to monitor these changes. The objective of this project was to demonstrate the applicability of HRR to deep subsurface problems, where the top of the sandstone formation was approximately 515 feet below ground surface. Additionally, it was expected that the contrasts in electrical properties between the Shannon Sandstone and injected fluid would be small, making the monitoring of the process very challenging.

The results of the test showed that HRR was able to monitor the changes in the electrical properties during the individual injection periods as well as over the entire run of the test. In both cases, the changes were subtle (4-5 times that of the measurement noise level), due to the small electrical contrast between the electrically conductive formation and the injected solutions. The HRR data could not differentiate Shannon water injections and the 1.5% (by volume) surfactant injections due to the minimal electrical difference between the two solutions. Flow directions and boundaries to flow were mapped electrically. HRR time series data also exhibited a classical response typical of hydraulic well test data.

Collectively, the HRR data suggest an explanation for the poor performance of the surfactant test, indicate hydraulic characteristics of the target reservoir, and offer possibilities for improving subsequent tests.

TABLE OF CONTENTS

EXECUTIVE SUMMARY 1

1.0 INTRODUCTION 3
1.1 Scope Of Work 3
1.2 Project Goals 4

2.0 BACKGROUND 4

3.0 SURFACTANT INJECTION TEST 7

4.0 HRR DATA COLLECTION 11
4.1 HRR Methodology 11
4.2 HRR Instrument Trailer 13
4.3 HRR Sensors 15
4.4 HRR Data Acquisition 16

5.0 TEST RESULTS 17
5.1 HRR Time-Series Analysis 18
5.2 HRR Analysis of Spatial Flow Characteristics 24
5.2.1 Two Dimensional HRR Contour Data (Injection Well 63S34) 25
5.2.2 Two Dimensional HRR Contour Data (Injection Well 65SX34) 28
5.2.3 Summary of HRR Analysis Of Spatial Flow Characteristics 31

6.0 CONCLUSIONS 34

LIST OF FIGURES

Figure 1: Project Area within the Teapot Dome Oilfield NPR-3. 5

Figure 2: Teapot Dome Oilfield Geologic Column at NPR-3. 6

Figure 3: Shannon Surfactant Treatment Project. 7

Figure 4: Water Production versus Time. 9

Figure 5: Oil Production versus Time. 10

Figure 6: Comparison of Oil to Water Ratios. 10

Figure 7: Layout of the HRR system Connected to Existing Infrastructure. 13

Figure 8: IT with Satellite Dish deployed at RMOTC. Injection Well #65SX34 in Background. 14

Figure 9: View Inside IT Trailer 14

Figure 10: HRR Electrodes Layout (150 m scale). 15

Figure 11: Oblique View of Site, Looking East & Nearly Horizontal. Top Layer Represents the Surface, Middle Layer is Top of Shannon, and Bottom Layer is Bottom of Shannon. 16

Figure 12: Raw HRR Time-Series Data at Several Wells During Current Application to Well 63S34 During Surfactant Flooding on Week 5 of the Test. Injection Periods Indicated by Vertical Lines. 17

Figure 13: Dimensionless Electrical Response from Receiver 63S34 from Transmission on Channels 1 to 11 During the Week of July 24 through 29, 2006 (Surfactant Injection Period). 19

Figure 14: Time Shifted and Stacked Electrical Responses from Figure 13. 19

Figure 15: Function Fits to the Critical Parts of the Averaged Electrical Response During the Surfactant Injection. 20

Figure 16: Example of Electrical Response on Four Wells During Fluid Injection Testing at the Hanford Site (from Barnett et al., 2004). 21

Figure 17: Slug Test Approximations with HGI Electrical Monitoring Data for Wells 63S34 & 65SX34. 24

Figure 18: Background Electric Field Relative to Injection Well 63S34 Prior to Surfactant Injections. 25

Figure 19: Changes in the Electric Field During Surfactant Injections for Injection Well 63S34. 26

Figure 20: Changes in the Electric Field After All Injections for Well 63S34. 27

Figure 21: Background Electric Field Relative to Injection Well 65SX34 Prior to Surfactant Injections. 28

Figure 22: Changes in the Electric Field During Surfactant Injection for Well 65SX34. 29

Figure 23: Change in the Electric Field After all Injections for Well 65SX34. 30

Figure 24: Summary of HRR Analysis of Spatial Flow Characteristics. 32

LIST OF TABLES

Table 1: Water Surfactant Injections 38

Table 2: Production Wells..... 39

Table 3: Water Analysis of Selected Test Wells..... 40

EXECUTIVE SUMMARY

hydroGEOPHYSICS, Inc. (HGI) and the Rocky Mountain Oilfield Testing Center (RMOTC) jointly conducted a test of HGI's patented High Resolution Resistivity (HRR) sub-surface fluid monitoring technology. HGI's RMOTC project demonstrated the use of a non-intrusive measurement method (HRR) to monitor sub-surface fluid movement during an enhanced oil recovery (EOR) project. The RMOTC EOR project, located at the Naval Petroleum Reserve No. 3 (NPR-3), was designed to evaluate the effectiveness of an EOR surfactant flood in the Shannon Sandstone.

HGI's technology effectively monitors spatial and temporal evolution of fluid migration in the subsurface. The monitoring technology relies on a special application of HRR using direct-current electrical geophysics to observe the changes in electrical properties during the injection and movement of water, steam, oil, carbon dioxide, surfactant, or any other sub-surface fluid. HRR is robust and easily deployed in a variety of settings, making it an attractive option for monitoring subsurface fluid movement in oilfield settings. The HRR system is non-intrusive since the monitoring system uses existing steel-cased oil wells as electrodes, controlled by an on-site remotely operated Instrument Trailer.

Project Objective **–** The principal objective was to demonstrate HRR technology for non-intrusive measurements to monitor sub-surface fluid movement during Enhanced Oil Recovery.

Injection Parameters **–** Two injection wells and four production wells were used to conduct the EOR flood. After 18 weeks of water and diluted (1.5%) surfactant injections, only two of the four production wells showed traces of increased oil production. The increased rates of production were less than one barrel of oil per day for both wells 73S34 and 84S34 for 4,605 bbls of injected water and surfactant. Such a small change spread over 122 days would not be expected to produce much of a change in any traditional monitoring method.

HRR Results **-**The test revealed that HRR has the ability to characterize the performance of the injection wells during a flood. HRR data for the injection wells (63S34 and 65SX34) showed a linear electrical response during injection and an exponential recovery (for the electrical data)

upon cessation of the injection. The calculated recovery time for well 63S34 was approximately 10 hours while well 65SX34 was approximately 1 hour. RMOTC personnel noted that well 65SX34 never attained significant back-pressure, whereas back-pressure was observed in well 63S34. The implication is that the HRR electrical recovery times could be used to determine the aquifer hydraulic recovery times. The rapid recovery time for well 65SX34 made it a poor choice for an injection well, while the much longer recovery time for well 63S34 indicates that it was more suitable as an injection well for the EOR. If HRR recovery time data had been available early in the test, well 65SX34 could have been eliminated, and another, more suitable injection well, selected.

Despite the negligible change in oil production, the HRR electrical monitoring system was able to identify subtle changes in spatial fluid flow characteristics and migration direction. Analysis of the HRR data showed little change in production character either during the surfactant injection period or shortly thereafter, suggesting that the surfactant flood had negligible impact on the hydrogeologic environment. Collectively, the HRR data suggest an explanation for the poor performance of the surfactant test, indicate hydraulic characteristics of the target reservoir, and offer possibilities for improving subsequent tests.

1.0 INTRODUCTION

In May 2006, hydroGEOPHYSICS, Inc (HGI) signed a CRADA with DOE's Rocky Mountain Oilfield Testing Center (RMOTC) to demonstrate the High Resolution Resistivity (HRR) technology for non-intrusive monitoring of fluid movement (water and surfactant) during an Enhanced Oil Recovery (EOR) test. The selected test site was the Shannon Sandstone reservoir in Section 34 of the Naval Petroleum Reserve No. 3 (NPR-3).

HGI, located in Tucson, AZ, has a patented[1] technology for monitoring the spatial and temporal evolution of fluid migration in the subsurface. The HRR technology exploits a unique application of electrical geophysics to observe time-dependent changes in subsurface electrical properties. Subsurface changes could be the result of a fluid injection which artificially promotes movement of a fluid (water, steam, oil, carbon dioxide, surfactant, etc.) through the subsurface. Currently, HGI uses the same technology to detect and monitor potential leaks that may occur from subsurface nuclear waste storage tanks at the Department of Energy (DOE) Hanford Nuclear Reservation in eastern Washington State.

1.1 Scope Of Work

The scope of the project included designing dedicated geophysical instrumentation capable of monitoring the electrical potential within a complex environment, deploying the instrument to the site, and acquiring geophysical data remotely for a period of 18 weeks. The site complexity was a result of the high degree of metallic infrastructure that could potentially interfere with electrical measurements, resident wildlife, and the subsurface geologic structure of the area.

The geophysical monitoring was accomplished by measuring the electrical potential on a series of 22 steel-cased wells using DC resistivity in a pole-pole array configuration. The measurement strategy incorporated the general philosophy of tomography, where one well was used to transmit current while the remaining wells measured the voltage. A measurement cycle was complete when each well had a turn at current transmission, which allowed the subsurface to be viewed from all angles. For this study, two of the geophysical monitoring wells were used as injection wells for the EOR test, four geophysical monitoring wells were production wells, and

[1]Patent #US 7,141,982, Estimation of Leakage Rates Using Voltage Measurements

the remaining were not actively used for the EOR flood. The two remote reference electrodes, for the pole-pole array, were located at least 8,000 feet away from the closest EOR injection well.

1.2 Project Goals

The main goal of the geophysical monitoring with HRR was to demonstrate that the technology was capable of tracking the fluid movement, including water, surfactant, and oil, as a result of EOR floods. The HRR method has been applied successfully in near-surface applications for underground storage tank leak detection. The extension of this test would show HRR's applicability to deeper problems that are typically encountered in EOR.

Success in the test was measured by the ability of the method to obtain quantitative and qualitative measures that describe the movement of fluids as a result of EOR floods.

2.0 BACKGROUND

The geophysical monitoring test was conducted at NPR-3, which is located approximately 35 miles north of Casper, Wyoming (Figure 1). The field is situated on the Teapot Dome Anticline in the Powder River Basin. The Teapot Dome is the southern extension of the much larger Salt Creek Anticline. Over 1,300 wells have been drilled into the Teapot Dome, of which approximately 700 are actively producing oil and gas from several different geologic formations. The most prolific oil production originates from the Shannon Sandstone (Goehring & Davidson, 2001) located from 400 to 1,200 feet below ground surface (Figure 2). Original reserves for the Shannon Sandstone were estimated to be approximately 144 million barrels of oil (MMBO). To date, only 11.4 MMBO have been extracted.

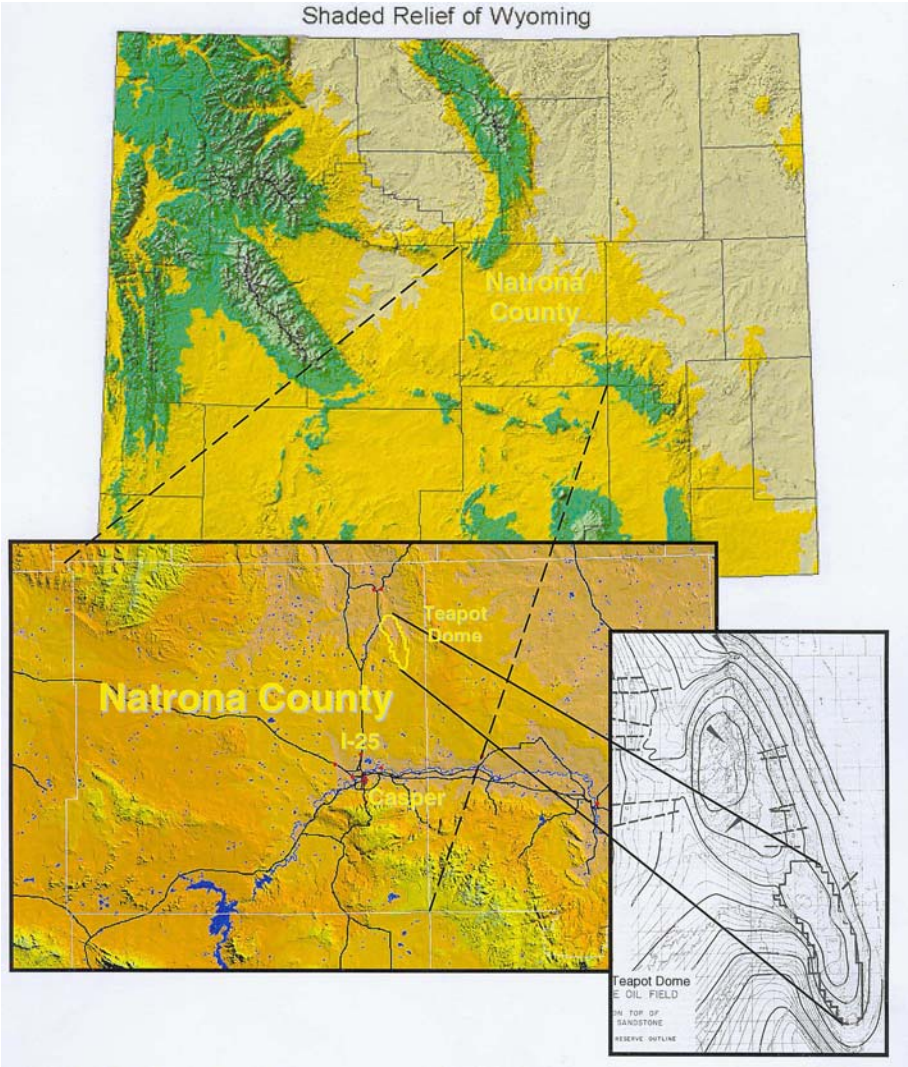

Figure 1: Project Area within the Teapot Dome Oilfield NPR-3.

Several enhanced oil recovery (EOR) and improved oil recovery (IOR) processes have been deployed within the Shannon Sandstone to improve oil recovery rates. These processes include waterfloods, steamfloods, and injection/soak/production operations (also called huff n' puff) where surfactant is injected into a well to build pressure before returning it to production. Steamflood operations began in 1985 and ran through the mid 1990s. Steamfloods were initially successful at increasing production in the Shannon, but problems with premature breakthrough of steam and the high costs to generate the high-quality steam necessary for successful implementation eventually forced abandonment of the project.

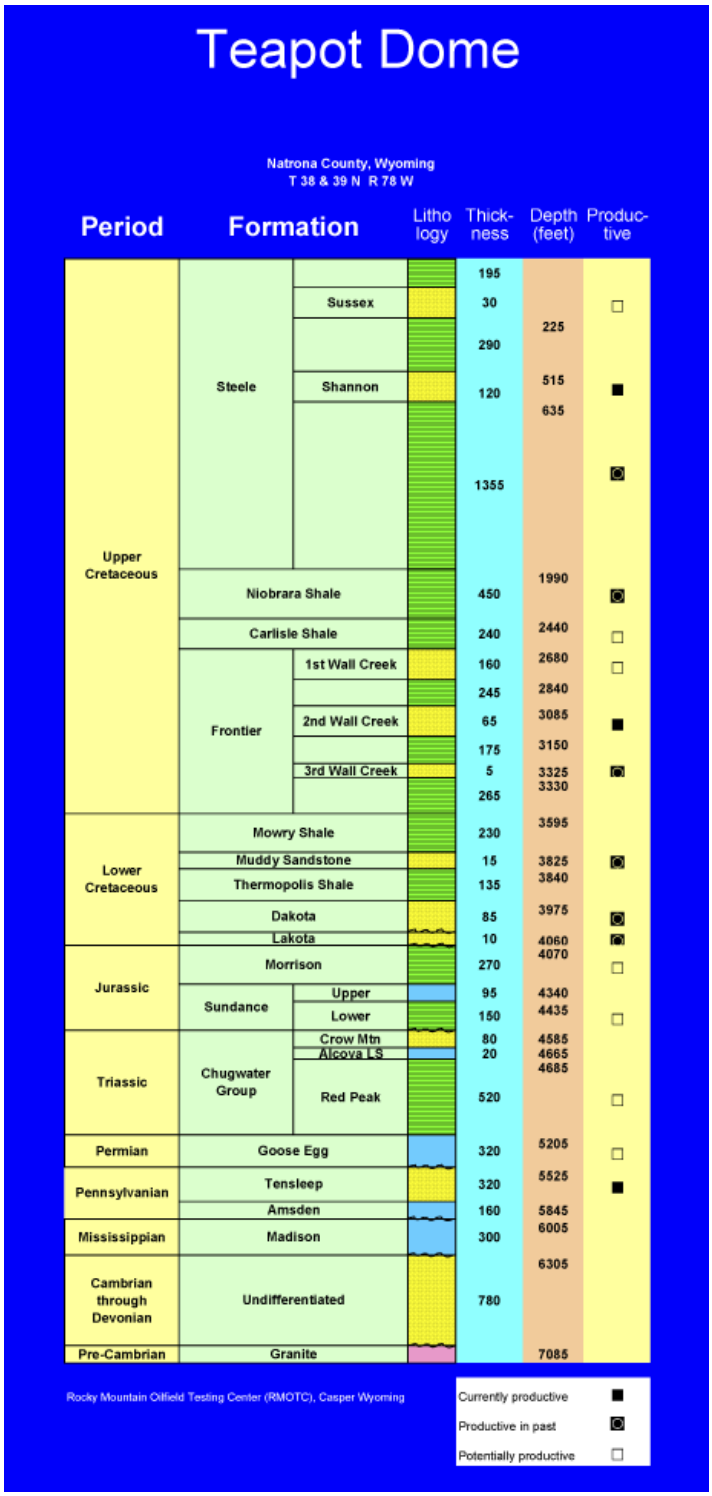

Figure 2: Teapot Dome Oilfield Geologic Column at NPR-3.

3.0 SURFACTANT INJECTION TEST

The geophysical monitoring was conducted during an EOR test of a dilute (1.5% by volume) surfactant. The objective of the EOR project was to treat a portion of the Shannon Sandstone reservoir in Section 34 of NPR-3 with a surfactant to mobilize residual oil. The concept behind the surfactant injection was that surfactant would "wet" the rock surfaces by reducing the surface tension between the water and rock interface, thereby facilitating greater efficiency in replacing the oil. In turn, the process would allow the oil to more easily move toward the four production wells.

The Shannon reservoir, a member of the Cretaceous Steele Shale Formation (Figure 2), is approximately 120 feet thick, with the top located ~500 feet below ground surface in this area. The project site was located within a structural compartment dipping gently to the NE and bounded on the north and south by curvilinear down-to-the-south normal faults striking ENE. The faults exhibit less than 100 feet of dip slip, and likely a small amount of strike slip. Fault planes typically dip about 45°-55° and are smeared with bentonitic clays. The clays were expected to seal the faults.

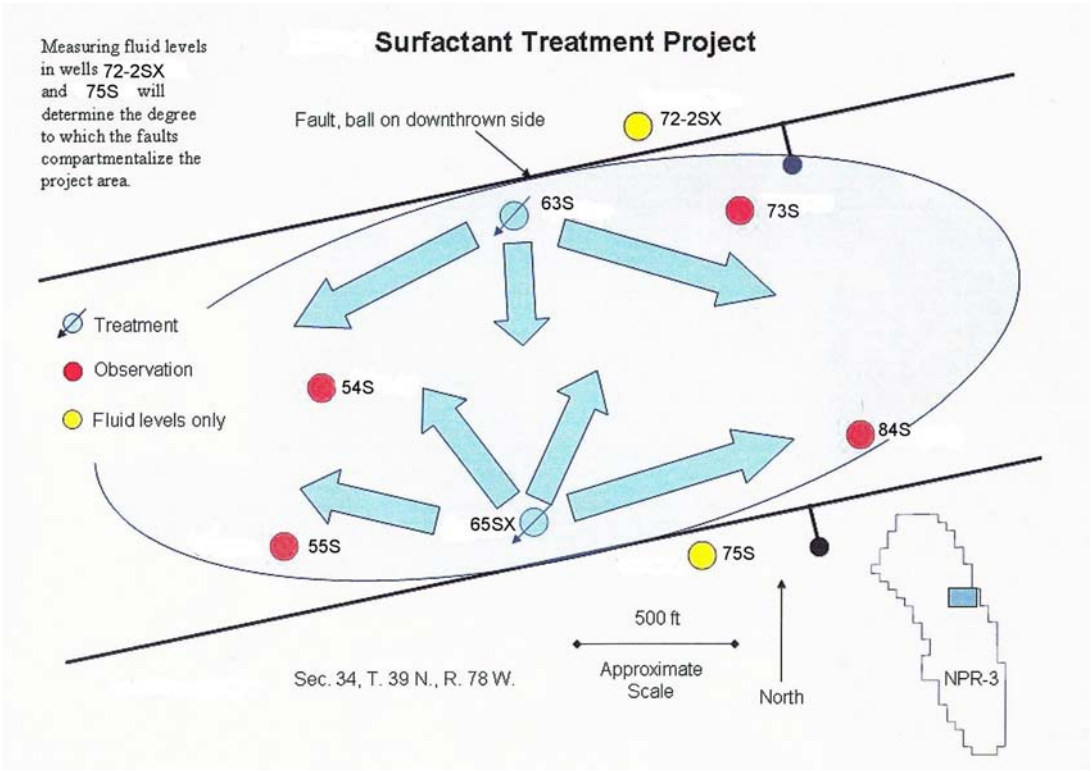

Figure 3: **Shannon Surfactant Treatment Project.**

The EOR procedure involved injecting fluid into one of two injection wells and extracting fluid from four nearby production wells. Figures 3 and 10 show the arrangement of wells used in the EOR test. The first series of injections, which started on June 26, 2006, included 4 weeks of water flooding, followed with 9 weeks of surfactant flooding, and ending on October 25, 2006, with the final 5 weeks of water flooding (Table 1). Each water injection consisted of 70 bbls from a locally derived groundwater source (Madison Formation). The surfactant flood included 1 bbl of surfactant mixed with 69 bbls of groundwater to create the 1.5% surfactant mixture. Floods were conducted weekly for four days (Monday through Thursday with one injection per day) followed by a 3-day off period. Weekly injections alternated between wells 65SX34 and 63S34.

Results - The effectiveness of the EOR test was evaluated by the production volume and oil/water ratios in the nearby production wells. Production well 73S34 was located 721 feet east of injection well 63S34, and well 84S34 was located 1,460 feet to the southeast. Production wells 54S34 and 55S34 were located 944 feet and 1,450 feet southwest, respectively (Figure 10). Production well 73S34 was located 1,340 feet northeast of injection well 65SX34 and well 84S34 was located 1,340 feet to the northeast. Production well 54S34 was located 880 feet northwest and 55S34 was located 760 feet west of 65SX34 (Figure 10). The product from the wells was analyzed for physical (amount of water and oil) and chemical makeup (Table 3). Figure 4 shows the water production for the wells during most of the EOR period from July 12 (HGI day 2385) to October 26, 2006 (day 2491). For reference, the surfactant injection occurred between July 24 (HGI day 2397) and July 29, 2006 (day 2402). Production data (Table 2) were reported individually for wells 73S34 and 84S34, whereas the production data from wells 54S34 and 55S34 were combined due to low values. Unfortunately, the physical property and chemical sampling of the production wells started after the beginning of the EOR test, so statistical background production levels weren't available to completely evaluate the effectiveness of the floods.

Figure 4 shows a relatively flat production rate with two short-duration anomalies. The first anomaly occurs at July 18 (HGI day 2391) for well 73S34 and is represented by two data points. The second anomaly occurs at September 21-22 (HGI days 2456-2457) for wells 73S34 and 54S34/55S34, respectively. The second anomaly is also represented by two data points; one for well 73S34 and one for the combination of wells 54S34/55S34 which are separated by a single

day. Interestingly, the second anomaly occurs at the very end of the surfactant test. Both anomalies are out of character for the general trends and no apparent explanation exists for the occurrence.

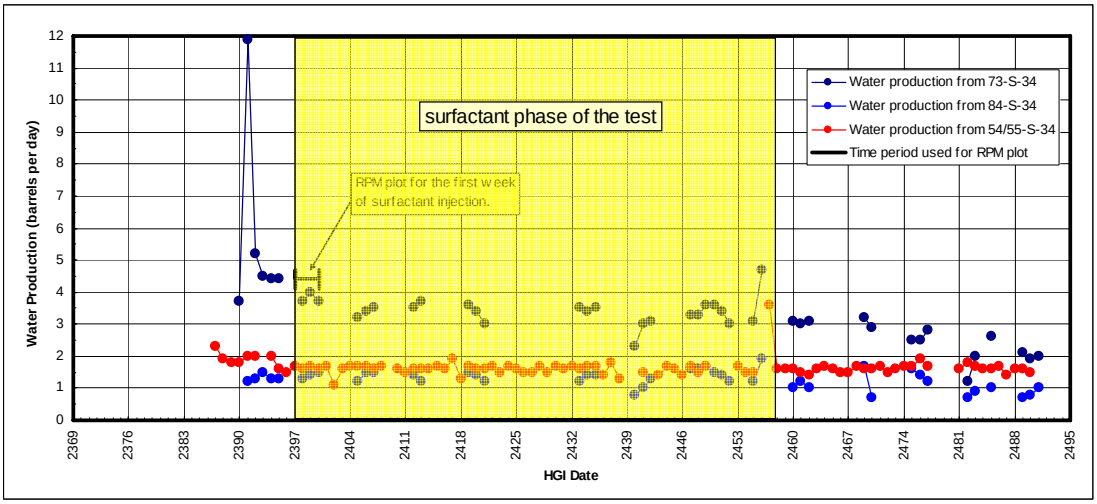

Figure 4: Water Production versus Time.

Other than the spikes in production, the general response for well 84S34 and the well combination 54S34/55S34 show a virtually flat trend for the duration of sampling. Well 73S34, however, shows a decline in water production over time. Of interest to the project is the oil production over the same time period. Figure 5 shows the equivalent plot of oil production over time. Note the expanded vertical scale. As with the water production data, the oil production data show relatively flat trends with a slight increase in oil production over time for well 73S34. However, during the same time period, well 73S34 shows a decrease in water production. In order to better view this possible relationship, a ratio of oil production to water production is shown in Figure 6.

Included in Figure 6 are linear trends representing the least squares fit to the oil/water ratios. All three linear trends show an increase in oil-to-water production over time, although the results for wells 54S34/55S34 are relatively flat, which suggests they may not be statistically significant. Wells 73S34 and 84S34 however, show distinctly positive trends suggesting that the EOR test was more effective at moving oil into these two wells (assuming a flat ratio before and after the testing period). Using the slope of the trends to evaluate effectiveness in the EOR test, well 84S34 was 6.6 times more productive and well 73S34 was 2.9 times more productive than the 54S34/55S34 combination.

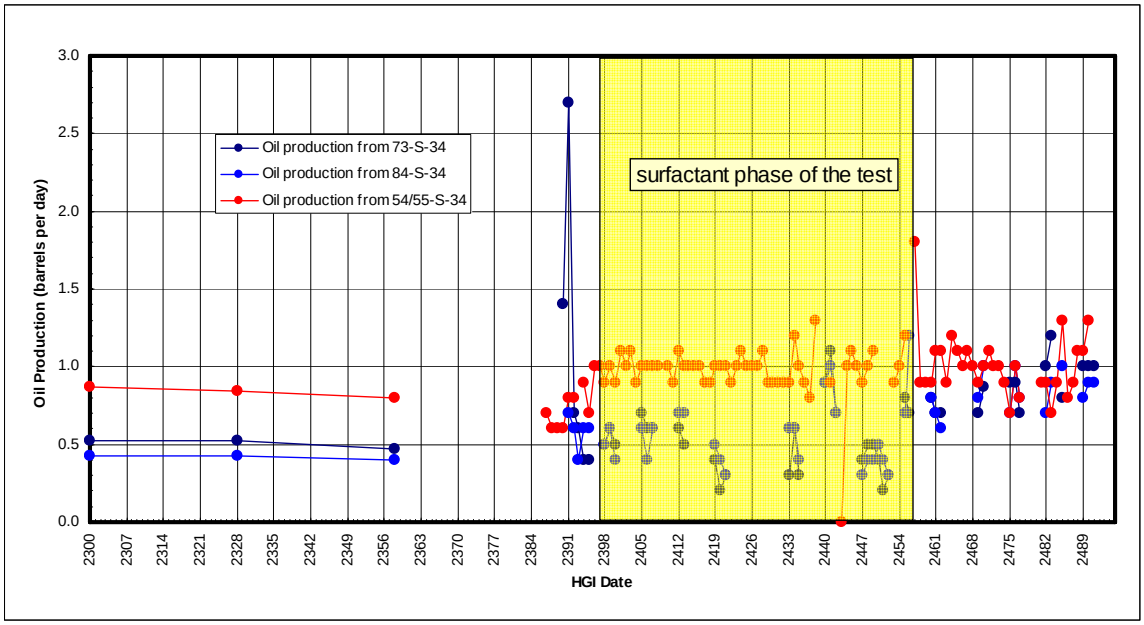

Figure 5: Oil Production versus Time.

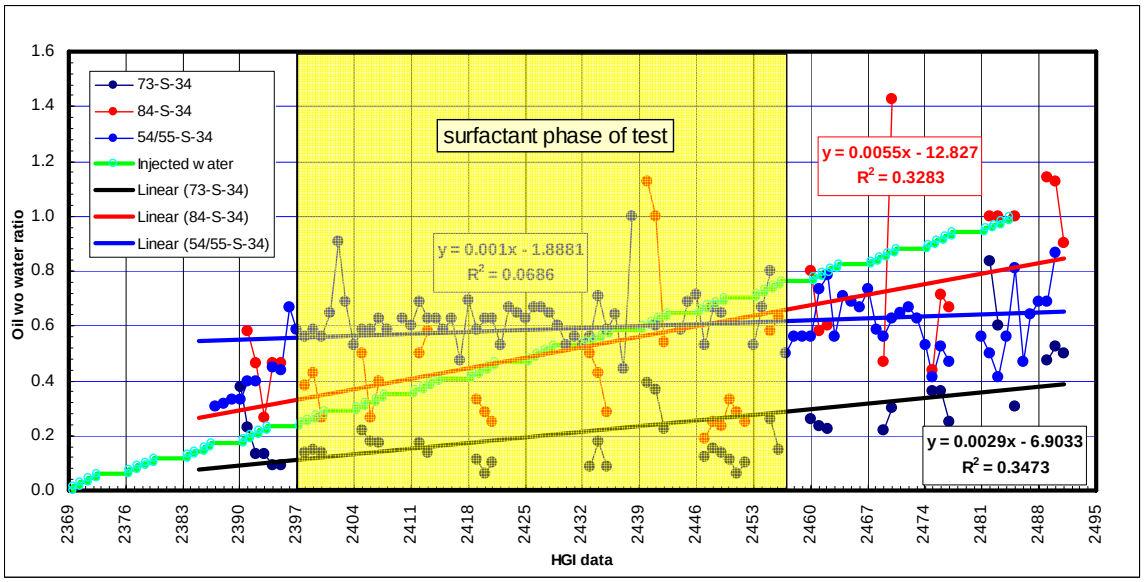

Figure 6: Comparison of Oil to Water Ratios.

Observations based on these analyses:

1) There doesn't appear to be any change in production character either during the surfactant injection period or shortly thereafter relative to the water-only phase. It might be concluded that the surfactant had no impact.

2) There is an interesting “ramp-up” for wells 54S34/55S34 at the onset of sampling. The change during this period of ramp-up is 0.007 bbls per day to 0.014 bbls per day. Obviously, at such low production rates, a small change can make a big percentage difference. What isn’t known is the average production (“background”) prior to the injection test, so it is difficult to put this into proper perspective. However, after the initial ramp-up, production tended to level off to a constant rate.

3) During that same time period, although again rather weakly represented, there appears to be a short term decline in the ratio for wells 73S34 and 84S34 at the onset of sampling. Unfortunately, no data were either gathered or provided for “background” or “baseline” production prior to, and during, the initial stages of the test. Such data would have been useful in putting the subsequent test results in better perspective. These two wells seemed to settle into a gently increasing production rate for the remainder of the test.

4) At the end of the test, the increased rates of production resulted in less than one barrel of oil per day for wells 73S34 and 84S34 for 4,605 bbls of injected water and surfactant. Such a small change spread over 122 days would not be expected to produce much of a change in any observational method.

5) Overall, there is a statistically demonstrable improvement in oil production in wells 73S34 and 84S34 although the gain in oil production was insignificant compared to the amount of water injected.

4.0 HRR DATA COLLECTION

4.1 HRR Methodology

HRR is a high density temporal and spatial sampling method that is ideally suited for EOR monitoring. The HRR method employs a four electrode array where one remote transmitter electrode and one remote receiver electrode are each placed far away from the monitoring area. The two remote electrodes may take the form of an array of stainless steel electrodes installed to a depth of 3 to 10 feet below ground surface, or may simply employ existing well casings. The connection to the “active” well casing electrodes moves within the test area. A transmitter current is driven between the remote transmitter electrode and a well casing electrode internal to the measurement area. The data system then cycles through all the

receiver electrodes measuring the voltage across the well casing electrodes and the remote receiver electrode. Data acquisition is multiplexed via HGI's data system in such a way that each well is used as a current transmission source and a voltage measurement location. Data are digitally sampled at programmable intervals to develop a time-series of electrical measurements. The evaluation of fluid movement is obtained by quantifying changes in the time-series electrical data.

By repeating the current transmission/voltage receiving procedure with other pairs of current electrodes in the well casing array, it is possible to calculate the spatial distribution of the electrical properties in the oil producing formation. The electrical properties depend strongly on pore fluid content and composition in the producing formation. Consequently, the HRR approach is particularly effective in providing information on the movements of oil, water, and gas - the principal fluids of interest in a petroleum reservoir. An important aspect of this method is that the oil well casings themselves are used as "long" electrodes (Figure 7).

The HRR methodology was deployed for use at Hanford, WA, where the issue of leaky underground storage tanks poses serious threats to the regional aquifer. The tanks were filled during the Cold War era with inorganic liquid waste with significant quantities of radiological and heavy metals. HGI's monitoring program commenced in early 2004 after three years of rigorous testing and two DOE-sponsored deployment evaluations. The HRR technology was evaluated against five other monitoring technologies and was found to produce data of higher resolution and greater sensitivity (by orders of magnitude) than the previously deployed technology.

HRR is robust and easily deployed in a variety of settings, making it an attractive option for monitoring subsurface fluid movement. The method relies on existing grounded metallic infrastructure around a site, including steel-cased wells, tanks, pipes, or metallic spikes. The incorporation of site infrastructure greatly reduces set-up costs. Specifically at Hanford, steel-cased monitoring wells surround each of the storage tanks and provide suitable sensors for monitoring changes in subsurface hydrogeologic conditions.

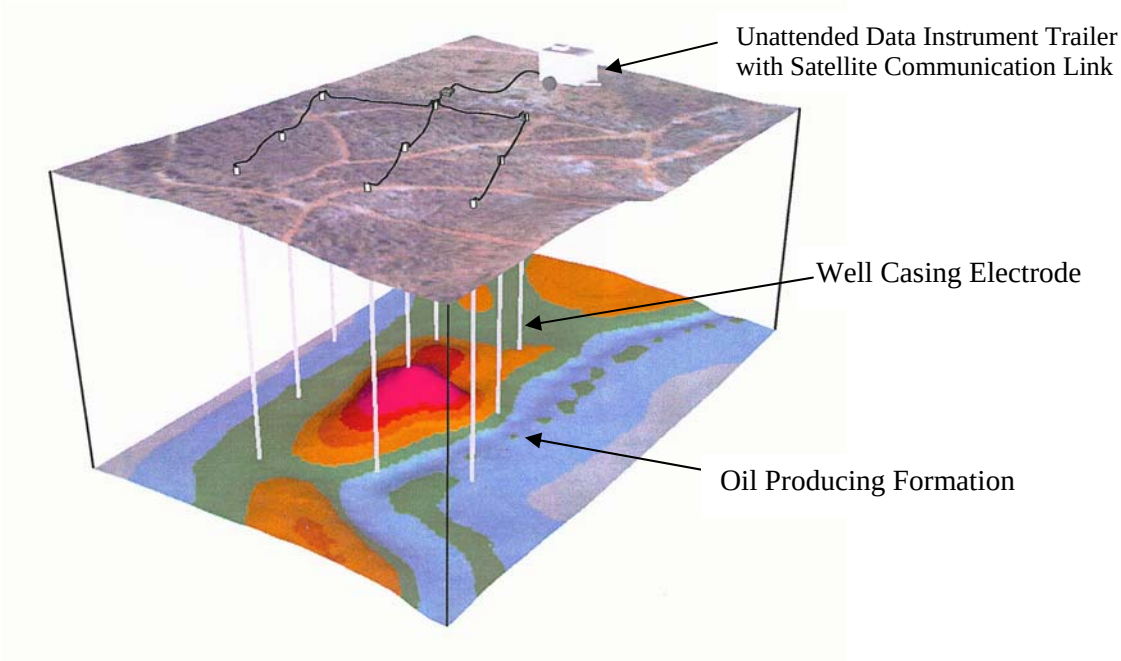

Figure 7:Layout of the HRR system Connected to Existing Infrastructure.

Another big advantage for HRR is that the method does not rely on inversion of data to obtain valuable information. Inversion is the process of calculating the spatial distribution of electric properties in the subsurface. All inversion routines for electrical resistivity geophysics are ill-constrained (small measurement noise can have large consequences on the final estimate), ill-posed (the number of measurements are much less than the number of grid cells for estimating the resistivity), and non-linear (must be solved iteratively by assuming a starting model). In certain situations, inversion can give excellent results and is the desired method of processing. However, where data are sparse, inversion can lead to large uncertainties in the results. HRR evaluates the measured data and can take advantage of any number of existing measurements.

4.2 HRR Instrument Trailer

Deployment of the HRR technology commenced in early June 2006, with the setup of the mobile Instrument Trailer (IT) at the RMOTC project site. Figure 8 shows the setup of the portable HRR IT equipped with a satellite communication link for data transmission and remote operations.

Figure 9 shows a view of HGI's custom-designed data acquisition equipment located inside the IT. The equipment includes a high capacity AC power subsystem, a backup power unit, a DC

power supply, transmitter, data acquisition computer, redundant data storage computer, and a data acquisition subsystem. The trailer also houses the remote communication system that allows all the hardware components to be accessed and controlled via a virtual private network (VPN) connection hosted over the satellite internet connection. The VPN system allowed data to be automatically forwarded to HGI's data processing facility located in Tucson, Arizona.

Figure 8: IT with Satellite Dish deployed at RMOTC. Injection Well #65SX34 in Background.

RMOTC site personnel provided assistance with the field deployment including: location of abandoned wells, electrically isolating adjacent well heads from monitoring wells, and installation of AC electrical power.

Figure 9: View Inside IT Trailer Showing 30-Channel Data System

4.3 HRR Sensors

The IT was connected to 22 steel-cased wells, including injection wells, production wells, and plugged or abandoned wells that were unused for EOR. In addition, remote transmitter and receiver electrode arrays were installed approximately 8,000 feet from the IT. Figure 10 shows the locations of the 22 steel well casings used for monitoring. The blue wells indicate injection wells, red wells indicate production wells, and green wells denote the balance of the 22 HRR monitoring wells. Approximately 50,000 feet of insulated electrical wire was used to connect the IT to the wells and the two remotes. Wires were buried under roads, in shallow trenches, and directly on the ground with a thin veneer of dirt for additional protection. Additional transformer wire was deployed in areas where wildlife (rabbits, rodents, etc.) were chewing wire insulation and breaking electrode wires.

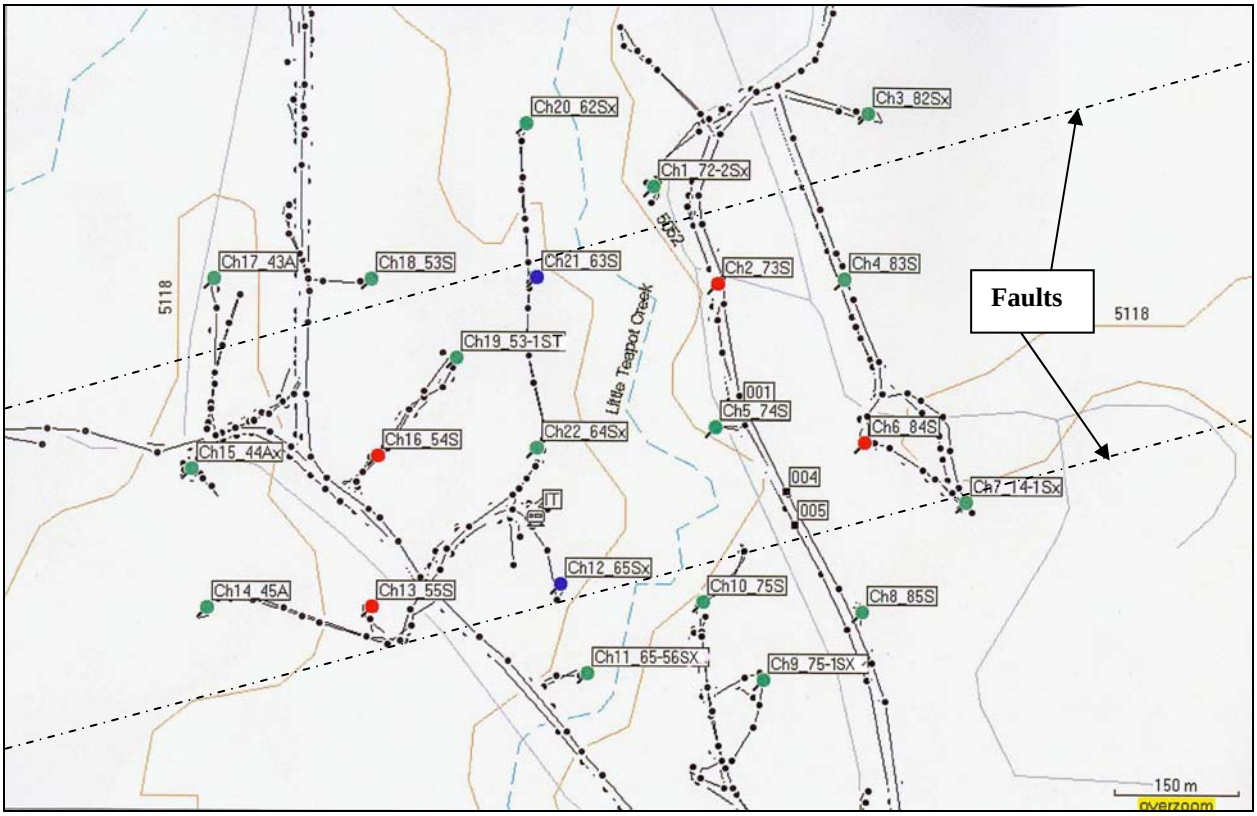

Figure 10: HRR Electrodes Layout (150 m scale).

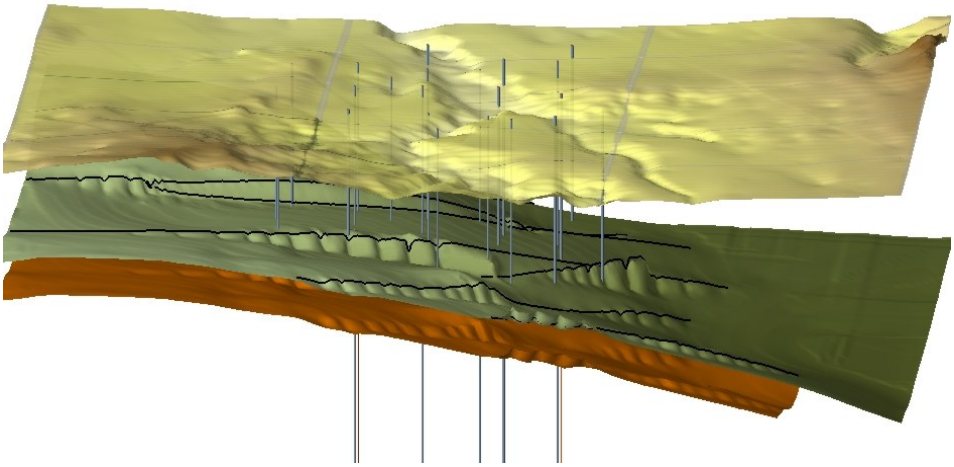

Figure 11: Oblique View of Site, Looking East & Nearly Horizontal. Top Layer Represents the Surface, Middle Layer is Top of Shannon, and Bottom Layer is Bottom of Shannon.

Figure 11 provides a perspective of the project site with respect to the Shannon sandstone. The top layer represents the topography of the surface. The bottom two layers represent the top and bottom of the Shannon sandstone, respectively. For scale, the HRR monitoring wells are shown penetrating through the Shannon with a minimum casing length of 660 feet (well 55S34) and maximum 3,125 feet (well 43A34).

4.4 HRR Data Acquisition

The 30-channel field data acquisition system acquired data almost continually, 24 hours/day with an 8-minute sampling rate. Each HRR data set consisted of voltage measurements from the 22 electrodes (oil well casings), providing a total of 462 measurements for each data set. Figure 12 shows an example time-series plot of HRR data during a surfactant flood. The figure plots transfer resistance (in ohms) for six receiver wells during current transmission on well 63S34. The exact periods of surfactant flooding are highlighted. The injection periods, where 70 bbls were pumped into the injection well, were usually less than 2 hours in duration and generally occurred in the morning. Gaps in the time-series resulted from extensive infrastructure failure due to wildlife (rabbits, rodents, etc.) damage to electrode wires.

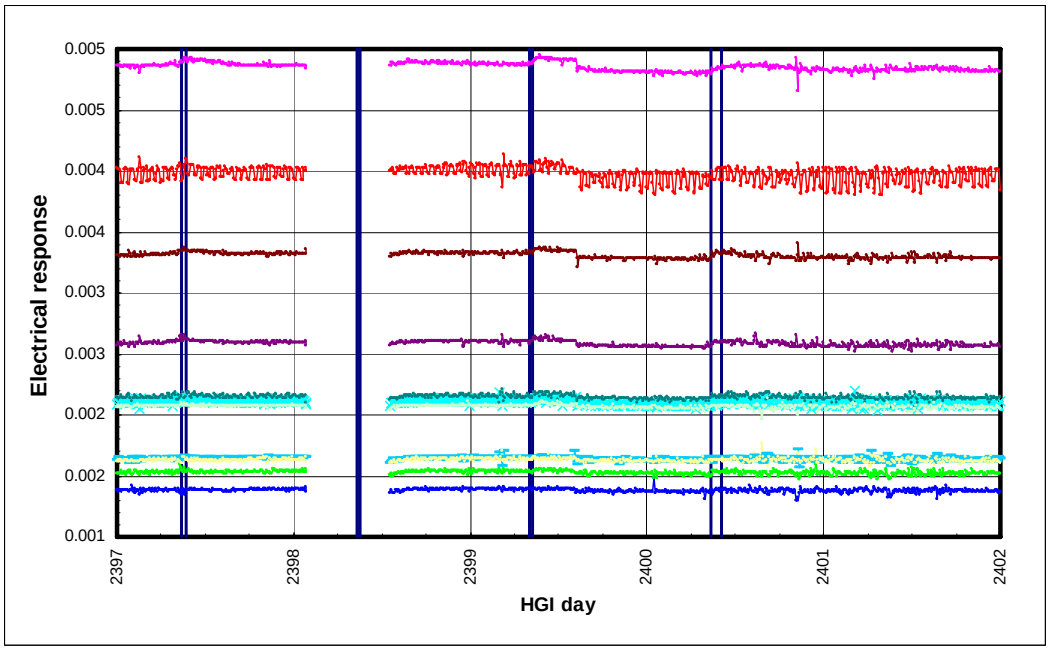

Figure 12: Raw HRR Time-Series Data at Several Wells During Current Application to Well 63S34 During Surfactant Flooding on Week 5 of the Test. Injection Periods Indicated by Vertical Lines.

The data in Figure 12 show that the subsurface is highly conductive. Resistance measurements between receiver wells and remote reference electrodes were on the order of several milliohms. The high conductivity of the subsurface made interpretation of surfactant flooding difficult immediately upon injection. In each of the receiver wells above, the resistance increased slightly. However, in some wells (in particular those with the lowest measured resistance), the increase in resistance was less than the noise level. The noise in the signal can arise from several sources, including diurnal temperature fluctuations and heating of wire, nearby electrical grounding, and general instrumentation noise. This level of noise would make traditional processing of electrical resistivity data, such as electrical resistivity tomography, very difficult. Time-series analysis is the only alternative to making meaningful interpretations of this data set.

5.0 TEST RESULTS

Time-series analyses were conducted on the HRR measurements to ascertain individual well responses to water flooding. The well responses were used to develop time constants that were interpreted as measures of pressure build-up in the reservoir. Increased pressure is needed to drive fluid (water-oil-surfactant mixture) towards the production wells. A secondary investigation of the data included a spatial analysis of potential fields.

5.1 HRR Time-Series Analysis

Figure 13 shows a sample of HRR time-series data in response to surfactant injections during week 5 of the test. The period in Figure 13 is the same as that of Figure 12. Four injections of 70 barrels/day (2,940 gallons/day) of fluid were completed on the mornings of Monday, July 24 (decimal day 2397) through Thursday, July 27 (decimal day 2400). For time reference, decimal day 0 equals January 5, 2000. Each surfactant injection lasted less than two hours and is represented in Figure 13 by vertical red bars.

The vertical scales of Figures 13 and 14 display the normalized, dimensionless units of "electrical response", with a background or equilibrium level at approximately 0.002 units. The dimensionless electrical response was created from the combined time-series data of transfer resistance measured from well 63S34 during current transmission on 11 wells. The 11 wells (located primarily east of the injection well) included those measured on channels 1-11 of the data acquisition system. In contrast, Figure 12 shows the individual transfer resistances of wells during current transmission on 63S34. The electrical response shows a linear increase during injection and an exponential decrease during recovery.

To compare the individual electrical response functions during the surfactant injections, each of the individual daily electrical responses were time shifted and normalized to produce an overlay plot. Figure 14 shows the results of this process and the striking similarity between the four injections. Each day's injection is indicated by a different color in the figure with the solid red line demonstrating the average of the four individual electrical responses. The use of the average electrical response allows fitting simple functions to segments of the data. Figure 15 shows the average response and two fitted functions; a linear fit to the brief injection window and an exponential fit to the longer recovery portion of the response.

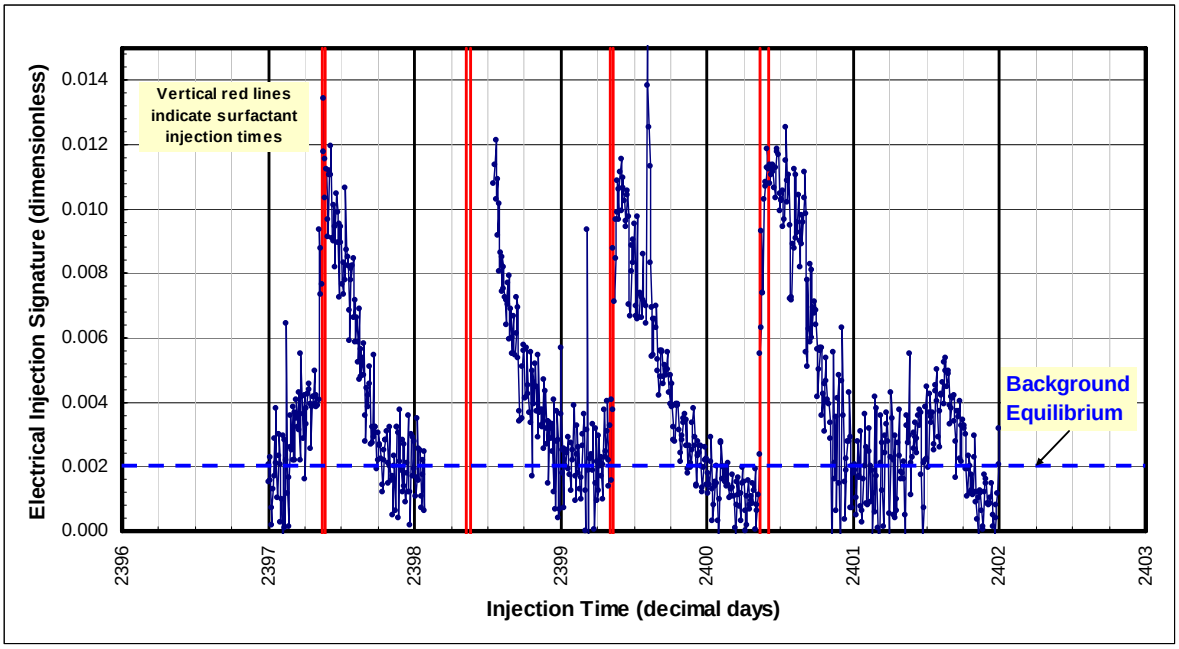

Figure 13: Dimensionless Electrical Response from Receiver 63S34 from Transmission on Channels 1 to 11 During the Week of July 24 through 29, 2006 (Surfactant Injection Period).

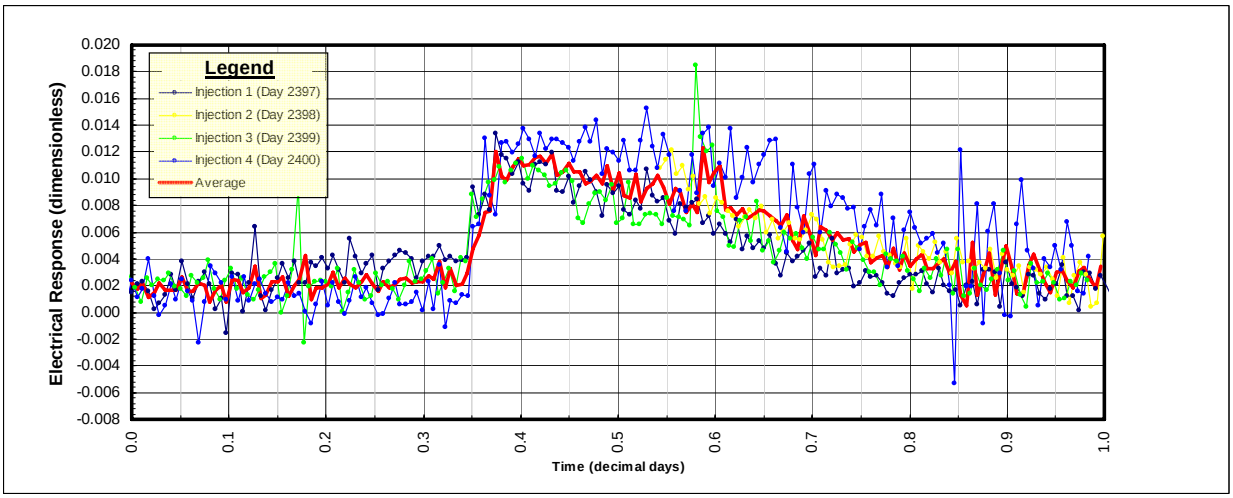

Figure 14: Time Shifted and Stacked Electrical Responses from Figure 13.

This linear electrical response to an increase in injection volume is well documented during HRR monitoring of several injection tests at the DOE Hanford Site (Barnett, et al, 2002; Barnett, et al, 2004; Burke, 2006; Schofield, 2006; Fink, 2007). Figure 16 shows the results of one Hanford leak injection test, where a very conductive fluid of sodium thiosulfate-pentahydrate was injected into an unconsolidated sandy gravel over several time periods within the 110-day test. Four wells were used to monitor the changes in electrical properties during the test and the figure

demonstrates the linear change during active fluid injection and exponential recovery. As long as the fluid injection volume is evenly distributed over the injection period, the electrical response should behave in this fashion, whether it is a shallow or deep application of the monitoring technology. The phenomenon was consistently observed during the HRR monitoring of the water and surfactant floods at RMOTC.

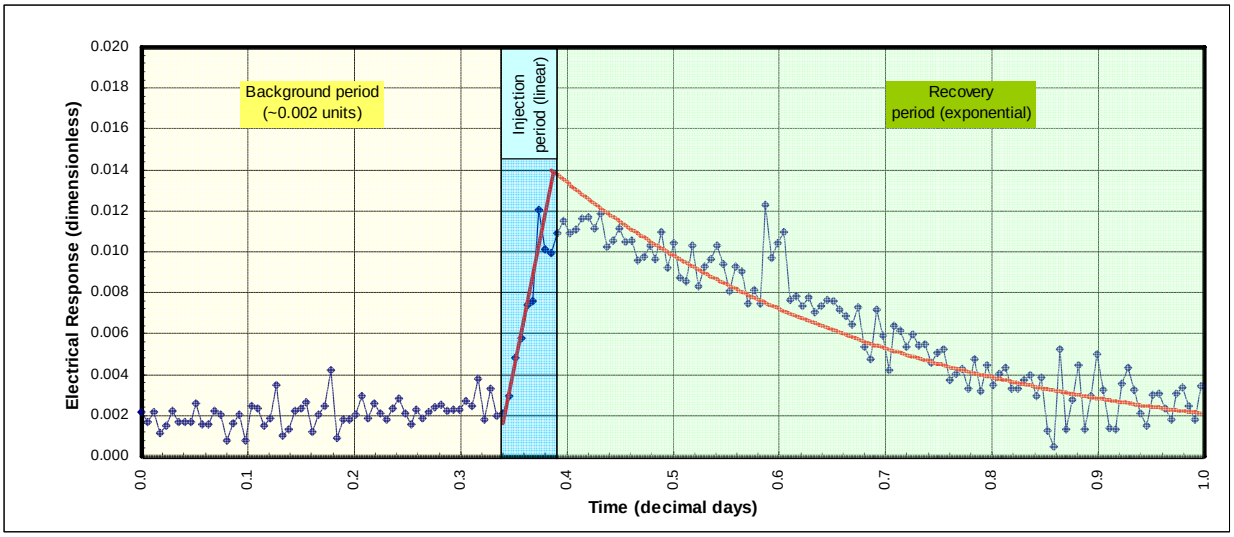

Figure 15: Function Fits to the Critical Parts of the Averaged Electrical Response During the Surfactant Injection.

At the end of the recovery period for each surfactant injection, the electrical responses returns to pre-test background levels, as shown in Figure 13. The post-injection return to the pre-injection level provides insight into the characteristics of the aquifer under testing conditions. Extensive evaluation of injection monitoring data at Hanford has shown that electrical recovery data will not return to pre-injection levels if the injection volume is large enough to create changes in the aquifer's electrical and hydraulic characteristics. Figure 16 shows a steady decrease in the overall trend for three of the wells demonstrating that the bulk subsurface electrical properties are changing. The electrical responses consistently returned to pre-injection levels for the RMOTC test indicating that the volume of water added was inconsequential in terms of the overall volume of the aquifer. This indicates that insufficient volume of water was used to result in a significant change in electrical conditions for individual injections. However, over the full term of the test, a small change in electrical properties was observed. This is discussed later.

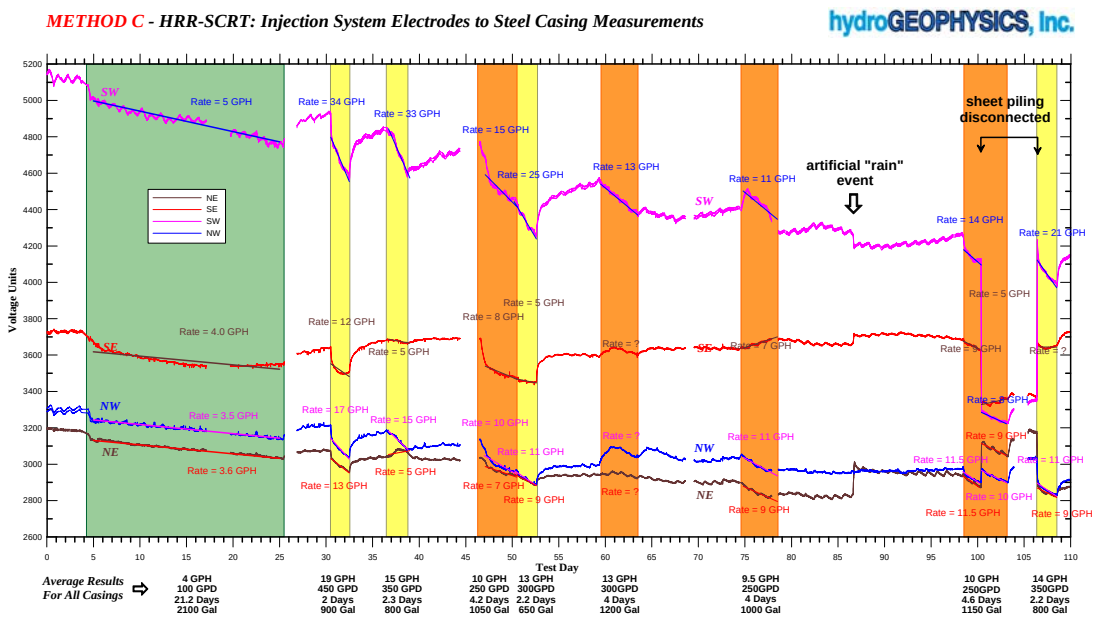

Figure 16: Example of Electrical Response on Four Wells During Fluid Injection Testing at the Hanford Site (from Barnett et al., 2004).

The exponential recovery in the electrical response for each injection is analogous to slug test analyses for hydraulic data. Previous testing at the Hanford Site has indicated that the termination of the linear injection period represents the equivalent of the maximum hydraulic head observed for a slug test. Assuming there is an electrical model equivalent for the recovery portion of the injection signature, the slug test methodology for aquifer evaluation was applied to the HRR monitoring data.

A hydraulic slug test involves inducing a rapid change in water level in a test well. By measuring and recording the rate of return to static conditions, it is possible to estimate the local horizontal hydraulic conductivity of the material surrounding the well. Slug test data are generally analyzed using relatively standard analytical solutions to the equations, which govern groundwater flow (Darcy's Equation). Homogeneity and constant aquifer thickness are common assumptions for conditions within the area of influence of the test. In practice, these are usually met because the radius of influence of most slug tests is fairly small.

Two classes of solutions are generally used in evaluating slug test data. The class of solutions, which includes the Bouwer and Rice and the Hvorslev Methods, relies on the assumption that water and soil are incompressible - that is, aquifer storativity is zero. This assumption allows the

use of a modified Thiem equation to predict well response. The potential which drives flow into or out of the well is expressed as a difference between head in the well and at a so-called "radius of influence." An alternate method of analysis includes the Cooper-Bredehoeft-Papadopulos method, which assumes a non-zero storativity. This method yields a solution analogous to the Theis equation for radial flow to a well.

For this analysis, the first class of solutions was used to evaluate the electrical data, where the analogous storage term from groundwater systems is assumed to be zero (i.e., no capacitance). According to Hvorslev (1951), the inflow rate at a well is proportional to the hydraulic conductivity and the potential difference in unrecovered head. The governing equation for the flow of injected water from the well into the aquifer is obtained from Darcy's equation:

$$q(t) = \pi r^2 \frac{\partial h}{\partial t} = FK\left(H - h\right) \tag{1}$$

where q is the flux rate, r is the well radius, K is the horizontal hydraulic conductivity, $(H\text{-}h)$ is the head difference in the well, and F is a shape factor, which depends on the geometry of the well intake and its location within the aquifer. If $q=q_0$ at $t=t_0$, $q(t)$ will decrease asymptotically toward zero at large times (Freeze and Cherry, 1979). Based on observations of the time dependence of head drop in the well after the slug of water was introduced, Hvorslev developed a time lag coefficient, τ_0:

$$\tau_0 = \frac{\pi r^2}{FK} \tag{2}$$

Conceptually, the time lag is defined as the time required for the induced head to drop to $1/e$ (37%) of its original value, and is a measure of the flux rate at which the additional volume of water enters the aquifer. When the time lag is introduced into Eq. (1):

$$\frac{dh}{(H-h)} = \frac{1}{\tau_0} \tag{3}$$

and the ordinary differential equation is solved with the initial condition of $h=H_0$ at $t=0$, one obtains:

$$\frac{H-h}{H-H_0} = \alpha e^{-t/T_0} \tag{4}$$

where t is the independent variable time and α is a lumped parameter constant containing the aquifer hydraulic characteristics. For the electrical measurements, the left hand side of Eq. (4) is

replaced with the averaged electrical response from each well.

Hydraulic data for the two injection wells (63S34 and 65SX34) were not available for analysis of aquifer properties. Therefore, the present analysis was limited to a comparison between measured electrical recovery times and theoretical hydraulic recovery times. Figure 17 shows the electrical recovery data for the two surfactant injection wells plotted in the format conventionally used for slug test analyses. The red and blue colored data points represent the averaged electrical responses observed as a function of time for the two wells 63S34 and 65SX34, respectively. The bold curves are exponential fits to the electrical data assuming an equivalent averaged electrical response starting point. In this case the starting point was 0.013. In general, an exponential response of the head (or in this case electrical response measured during head drop) suggests an over-damped recovery (Fetter, 2001). This type of recovery is characteristic of media with lower hydraulic conductivity.

The derived electrical recovery times, τ_0, for each well in Figure 17 are substantially different. Well 63S34 shows approximately 10 hours of recovery time, while well 65SX34 recovered within approximately 1 hour. During injections, well 65SX34 never attained significant back-pressure, whereas back-pressure was observed in well 63S34 (verbal communication RMOTC personnel). This visual observation adds significant support to the process used for deriving recovery times from electrical data. It is therefore interpreted that the electrical recovery times represent aquifer hydraulic recovery times.

The rapid recovery time for well 65SX34 made it a poor choice for an injection well since the success of the injection is controlled by the amount of head that can be generated within the reservoir. If insufficient head is generated, then oil cannot be driven towards the production wells. One reason for insignificant back-pressure in well 65SX34 is the screened portion of well appears to either cross, or be in close proximity to the known south boundary fault for the reservoir. It is likely that the fluids migrated directly into the fault, thereby reducing the well's performance in the EOR effort. In contrast, the much longer recovery time for well 63S34 indicates that it is more suitable as an EOR injection well.

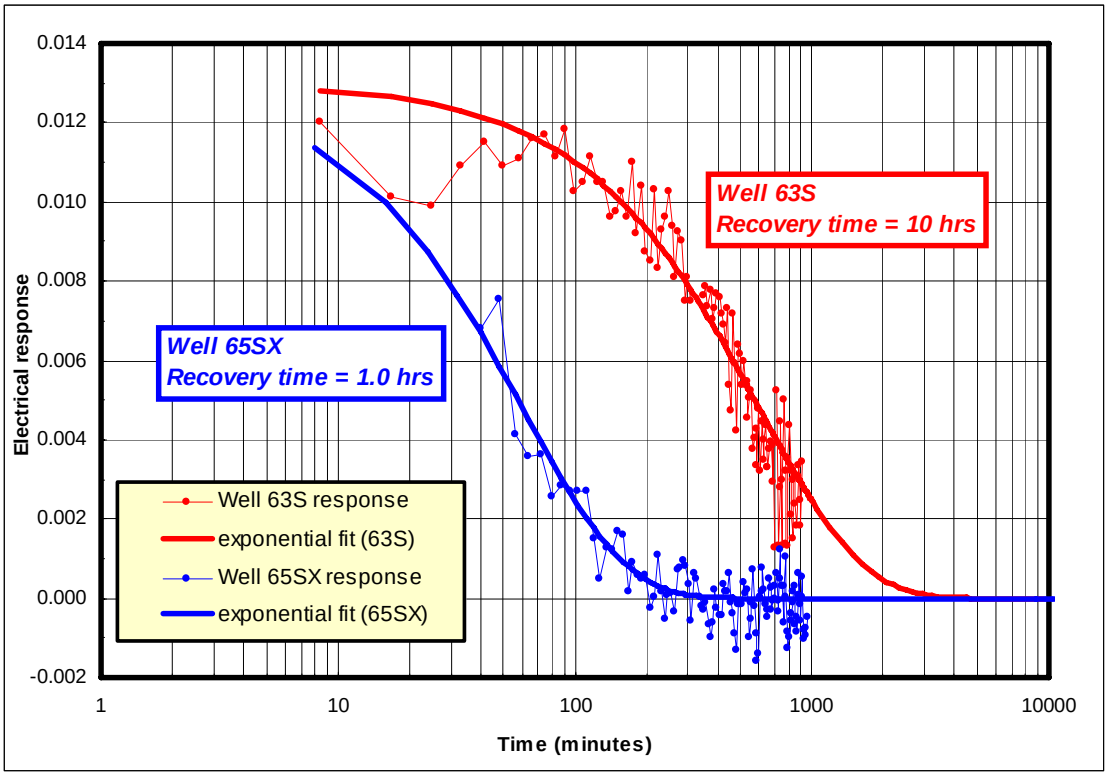

Figure 17: Slug Test Approximations with HGI Electrical Monitoring Data for Wells 63S34 & 65SX34.

5.2 HRR Analysis of Spatial Flow Characteristics

Two dimensional (plan view) contoured representations of HRR electrical data, acquired prior to and during the fluid injections, were generated to provide analysis of the spatial flow changes caused by the fluid injections. Two time periods of spatial flow characteristics were evaluated. This first centers around the time-series analysis evaluated in Section 5.1 (Figures 18 & 21), i.e. immediately before the surfactant injections. The second period evaluates the entire EOR test.

The spatial flow characteristics are evaluated by calculating the residual potential field. The residual potential field is calculated by removing a predicted primary potential field from the measured data to leave residuals, or changes from a background condition. Figure 18 shows an example of the distribution of the background potential field, where well 63S34 was the current transmission well immediately before surfactant injections. The remaining wells measured the voltage. Under homogeneous conditions, the field would drop off as a function of 1/r from the current transmission well, where r is the distance from the well. Figure 18 shows some deviation from this homogeneous assumption indicating some electrical heterogeneities. The offset of the

maximum response to the north of well 63S34 is likely due to either (or both) an electrically conductive body (possibly something structural) extending to the north or the well is not vertical and deviates to the north. This latter effect would imply that the hypocenter of the source is displaced to the north and perhaps very slightly to the northeast. This effect has been observed in other data sets, where wells were known to deviate.

Although the geologic structural boundaries (faults) for the Shannon Sandstone exist within the electrical mapping area, there is no obvious distortion of the electrical primary field that might suggest a structural influence.

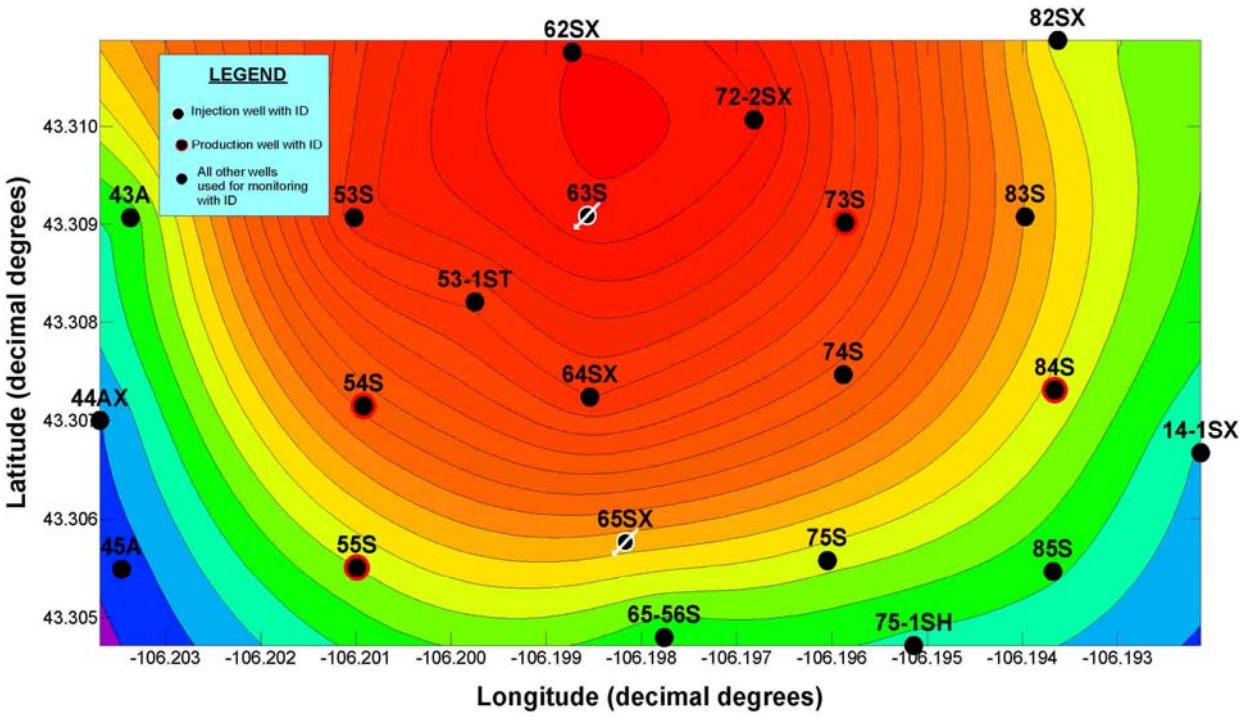

Figure 18: Background Electric Field Relative to Injection Well 63S34 Prior to Surfactant Injections.

5.2.1 Two Dimensional HRR Contour Data (Injection Well 63S34)

Figure 19 shows the residual potentials (after background field subtraction) in the electric field after the completion of 5 weeks (24 to 29 July). The exact values of the color scale are not important, and the colors are used simply to show relative changes. Warm colors (reds) represent the largest residuals, while the cool colors (blues) represent the smallest residuals. The maximum response is centered on well 63S34 because it was used as the transmitting source during surfactant flooding. However, there is a subtle northwest-southeast elongation to the electric field that may indicate preferential flow directions. There is little outside information to

verify this and the trend is sufficiently subtle that it may not be significant. It is noteworthy that production well 73S34 showed an unusually high volume of water production during the week immediately prior to the acquisition of these data. Additionally, the weak electrical responses at production wells 54S34, 55S34, and 84S34 are in accord with minimal water and oil production at those wells.

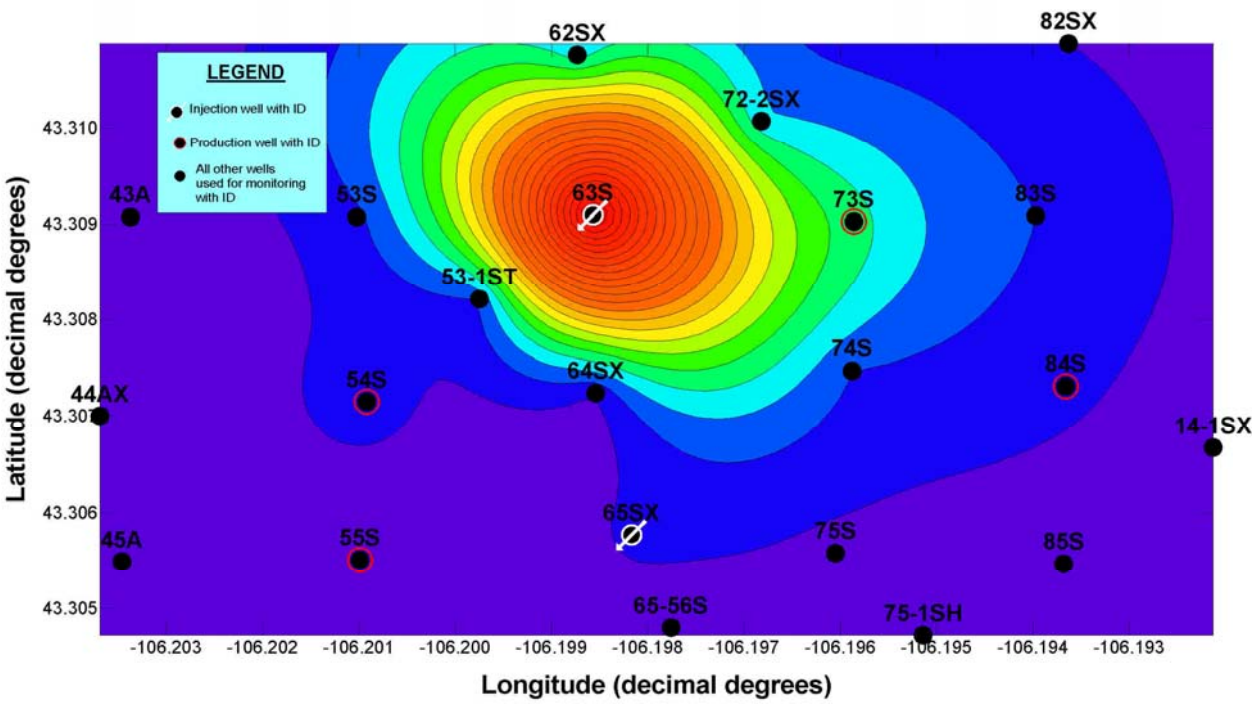

Figure 19: Changes in the Electric Field During Surfactant Injections for Injection Well 63S34.

Figure 20 shows the change in potential field between the start and the end of the entire EOR test, when well 63S34 was used as the current transmission well. The time period between background calculation and residual potential mapping is 122 days. The color scale represents the relative degree in residual potentials, where warm colors are residual values greater than the background (i.e., more electrically resistive) and the cool colors represent residual values less than the background. The zero residual is shown for reference. Volumetrically, any accumulation of water and surfactant should cause a reduction in the field, i.e., make the subsurface more electrically conductive. Conversely, any areas where injected solution does not readily flow should show up as relative increases in residual values.

It is immediately obvious that a large area of low residual potential occurs around and to the north of well 73S34. Well 73S34 reported the highest water production of all four production

wells. The combination of higher water production and lower transfer resistance would appear to be correlated. This suggests a general flow path away from the targeted portion of the Shannon reservoir to the north. The extent of the low transfer resistance to the north may explain the fluid migration path of water and surfactant injected into well 63S34. Based on this interpretation, water production in wells 72-2SX34 and 62SX34 would be expected to be higher.

The northern fault indicated by the thick black line doesn't appear to have any conspicuous influence on the fluid flow pattern. If this assumption is true, then the northern fault would have a permeable horizon at the equivalent depth as the Shannon, which would allow fluid to flow to the north across the fault. On the other hand, the southern fault and the weak low associated with injection well 65SX34 suggest a correlation between it and the southern fault.

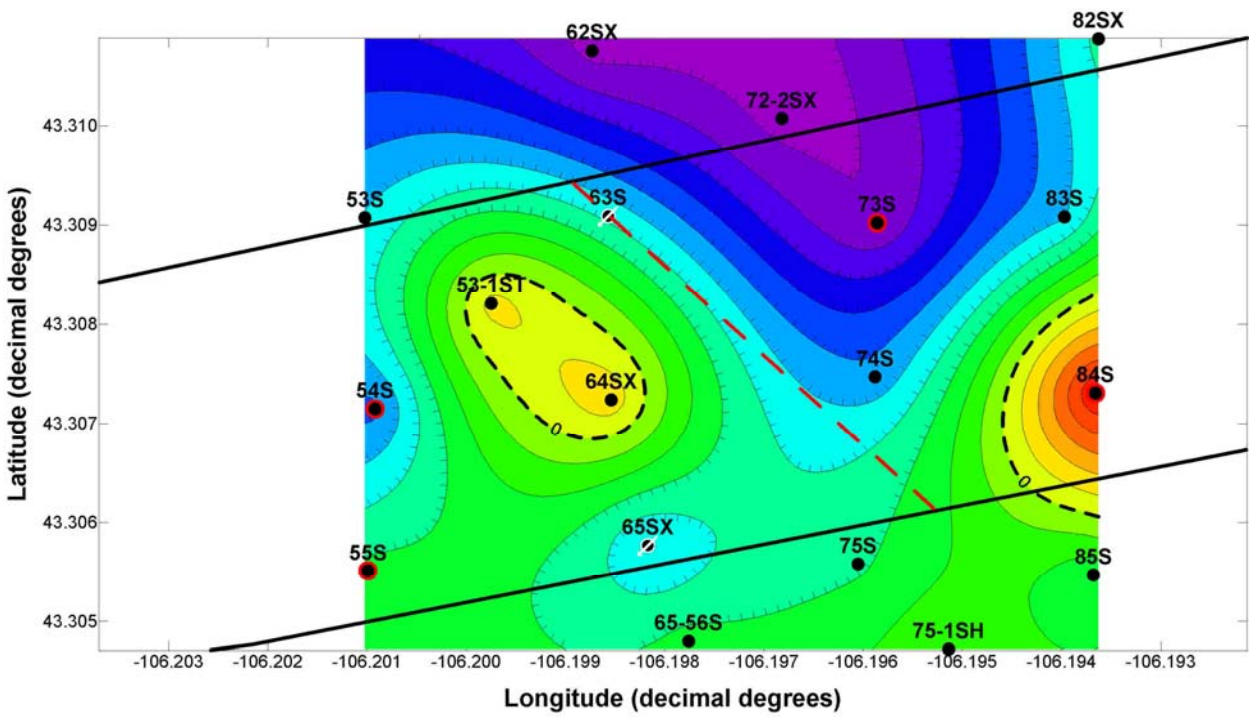

Figure 20: Changes in the Electric Field After All Injections for Well 63S34.

Well 84S34 showed the largest increase in oil production of all the wells. However, it did not show any change in water production, which may explain the residual potentials higher than 73S34.

Lastly, a dashed red line trending southeast-to-northwest was placed in the domain to indicate an electrical boundary, which in turn could be used to identify a hydraulic boundary. The boundary is interpreted as a change in intrinsic permeability and could be due to either a fault or a facies

change. Although a fault was not indicated on the Shannon structural map, the offset is parallel to the Shannon structural dip, which would make it less obvious in borehole data. The structural map does show this area bracketed by two wedge-shaped segments that appear to have hinge-like offsets relative to the target structural block. Alternatively, a facies change in the Shannon at this location might also produce the same effects although a change in facies would be expected to have considerable lateral extent.

5.2.2 Two Dimensional HRR Contour Data (Injection Well 65SX34)

Figure 21 shows the background potential field with well 65SX34 used as the electrical excitation source. The data were obtained immediately prior to surfactant injections. The results show a slight flattening of the electric field between wells 53S34 and 72-2SX34 that may represent the structural fault in that area. However, the feature is quite subtle and difficult to substantiate.

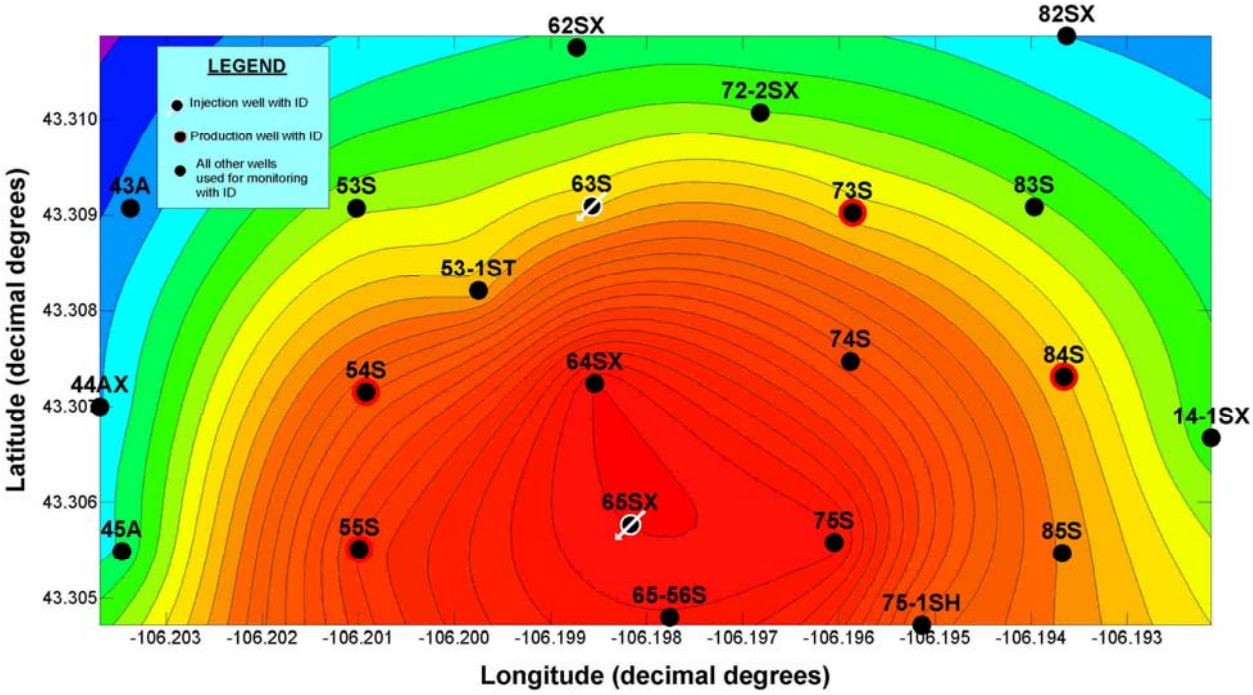

Figure 21: Background Electric Field Relative to Injection Well 65SX34 Prior to Surfactant Injections.

Figure 22 shows the residuals in the electric field after the completion of 5 weeks (24 to 29 July). The color scale is identical to the description in Figure 19, and the spatial distributions of the residuals are likely due to the presence of injection water. The maximum response is centered on

well 65SX34 because it was used as the transmitting source. There is a highly pronounced northeast-southwest orientation of the changes in the electric field that may indicate preferential flow directions. This orientation appears to agree with the known structural trends within the electrical mapping area.

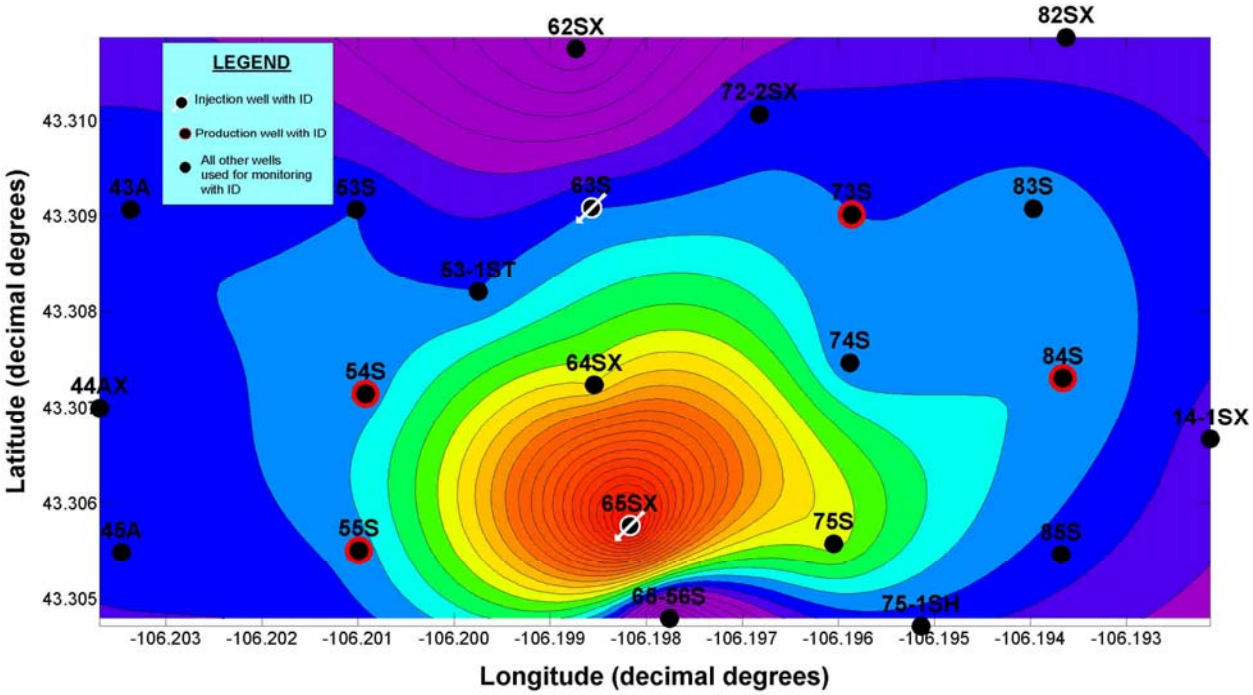

Figure 22: Changes in the Electric Field During Surfactant Injection for Well 65SX34.

Two additional anomalies occur at wells 65-56S34 and 62SX34 on the southern and north boundary, respectively. Electrical data recorded from both wells displayed inverted responses comparable to those indicated at other locations associated with localized electrically conductive features. The sharp gradient between injection well 65SX34 and 65-56S34 is interpreted to indicate the presence of the fault and that the fault exists in close proximity to the injection level in well 65SX34. The inverted response in well 62SX34 is interpreted to represent a localized conductive feature that is coincident with the northern bounding fault in that area. The fact that the faults appear to show up readily in the data for well 65SX34 and not for well 63S34 suggest a substantial difference in the well-to-fault geometry for the two wells. The stronger response associated with well 65SX34 seems to indicate a greater proximity to the southern bounding fault than 63S34 is to the north bounding fault. This interpretation is supported by the much shorter aquifer recovery time discussed in the Section 5.1. Spatially, the electrical responses at the four

production wells are nearly equal and would appear to agree with the negligible change in oil and water production at those wells.

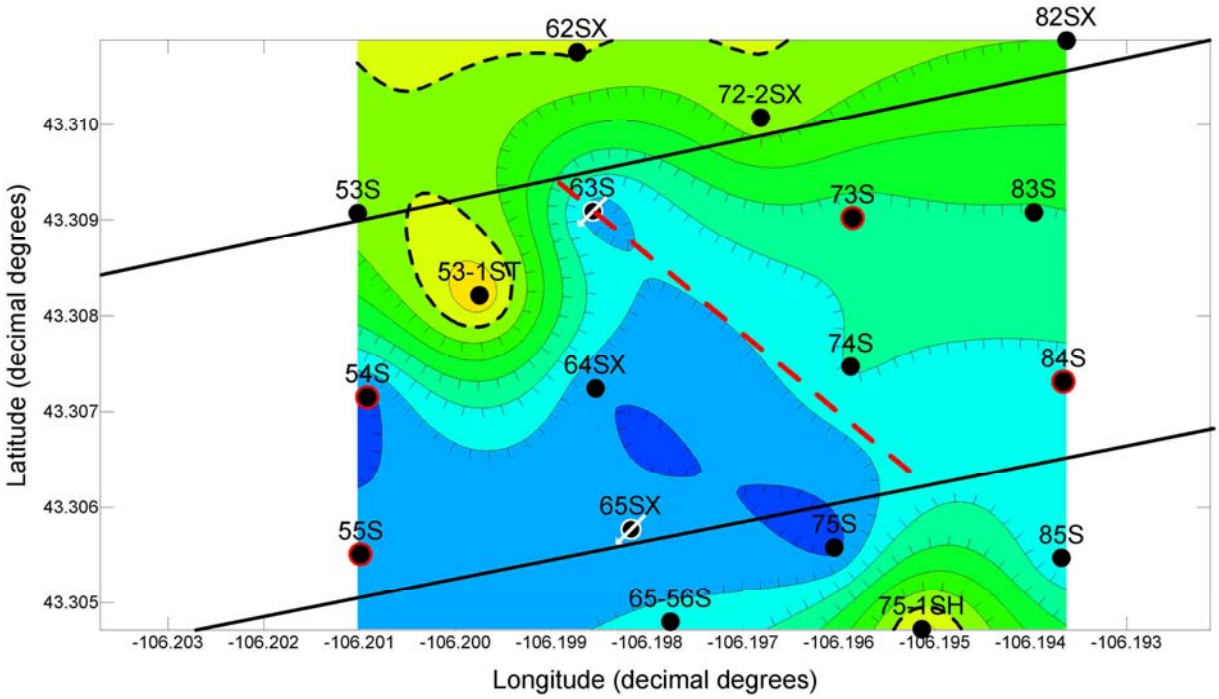

Figure 23: Change in the Electric Field After all Injections for Well 65SX34.

Figure 23 shows the change in transfer resistance between the start and the end of the test as observed relative to well 65SX34 (used as current transmission well). The description of the data and figure generation is the same as Figure 20. The lower residual potentials are now associated with well 65SX34 to the south. Note, however, that the magnitude of the lows is much less than those associated with well 63S34. The magnitude difference suggests that less fluid has accumulated in the Shannon reservoir in this area. It is likely that much of the fluid migrated down the southern fault. The highly permeable fault prevented pressure build up in the well, thereby reducing the effect of production on wells 54S34 and 55S34.

As with the results from well 63S34, the data from well 65SX34 also suggest a southeast-northwest trending barrier (indicated by a dashed red line in Figures 20 and 23). This trend, as drawn, strikes N50°W but is simply an approximation of the general trend indicated in both

figures. The majority of the strike directions mapped by Goehring and Davidson (2001) correspond with the hinge parallel faults of Cooper et al (2001). Additionally, the strike direction corresponds to the bedding plane of the Shannon and the general trend of the Teapot Dome anticline. Note that the majority of the low values are now to the west of the interpreted barrier. The interpreted barrier in both datasets appears to truncate against the north fault and perhaps against the southern fault.

5.2.3 Summary of HRR Analysis Of Spatial Flow Characteristics

Two dimensional (plan view) contoured representations of HRR electrical data, acquired prior to and during the fluid injections, provide qualitative information regarding the changes in the electric field caused by the evolution of the injected fluids. Such changes in the e-field are directly related to the injected fluid. Three time periods of spatial flow characteristics were evaluated, the results of which are summarized in Figure 24.

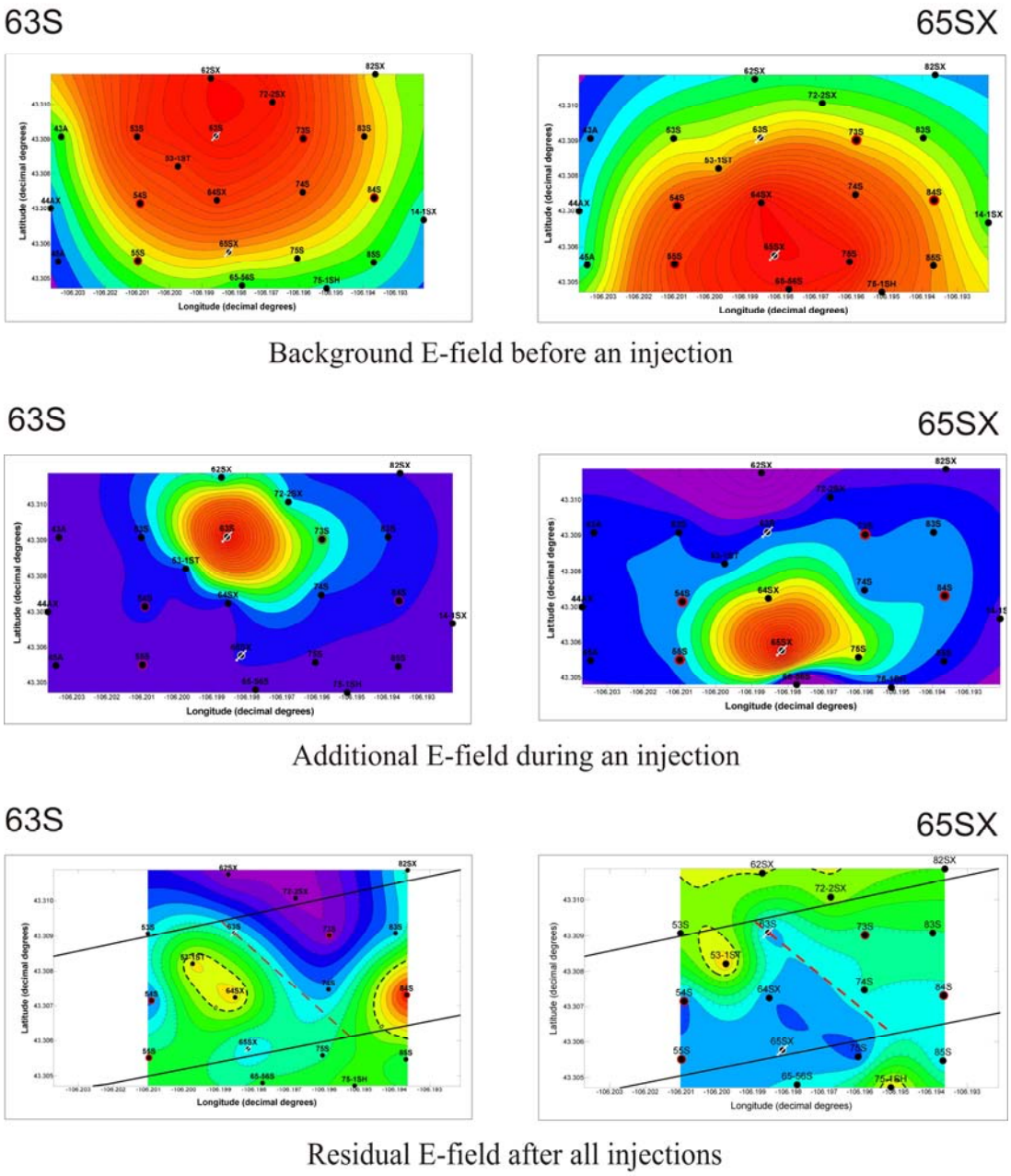

Figure 24: Summary of HRR Analysis of Spatial Flow Characteristics.

Figure 24 shows the six images already presented in Section 5.2 but as a single figure for ease of viewing. The images from top to bottom represent *before*, *during*, and *after* conditions for the two injection wells as labeled. The *before*, *during*, and *after* conditions are explained as follows:

> ***Before:*** This period represents the quasi-static conditions existing just before an injection. It is equivalent to background. These plots represent the e-field produced as a

result of energizing each of the injection wells immediately before an injection.

During: This period centers around the time-series analysis evaluated in Section 5.1 and represents the change in e-field (relative to *before*) as a result of the additional fluid being injected. ***These plots represent the dynamic conditions observed during injection.***

After: This period follows after all injections have been completed and the maximum amount of fluid has been injected and should still be near its source. The presence of the additional volume of injected fluid alters the overall transfer resistance observed from May through October.

6.0 CONCLUSIONS

1. **HRR electrical recovery time can be used to estimate oil well hydraulic recovery time.**

   A significant result of the HRR electrical response was the ability to perform a detailed assessment of performance for the injection wells. HRR data were used to derive a recovery time for each injection well. Results from these tests showed that wells (63S34 and 65SX34) exhibited a linear electrical response during injection and an exponential recovery. These visual observations add support to the process used for deriving recovery times from electrical data. The analysis showed that the two injection wells exhibited substantially different performance. Well 63S34 showed approximately 10 hours of recovery time, while well 65SX34 recovered within approximately 1 hour. The calculated recovery times were supported by verbal verification (RMOTC personnel) that well 65SX34 never attained significant back-pressure, whereas back-pressure was observed in well 63S34.

2. **HRR can provide a method to evaluate the suitability of injection wells before a long term EOR injection program is undertaken.**

   The rapid recovery time for well 65SX34 made it a poor choice for an injection well since the success of the injection is controlled by the amount of head that can be generated within the reservoir. If insufficient head is generated, then oil cannot be driven towards the production wells. Had the HRR data been available early in the EOR test, well 65SX34 might have been eliminated, another well selected, and the outcome might have been more useful as far as testing the effectiveness of the surfactant.

3. **HRR can provide a method to evaluate the optimal flood volume necessary for a successful EOR project.**

   Extensive evaluation of injection monitoring data at other evaluation sites has shown that electrical recovery data will not return to the pre-injection levels if the injection volume is large enough to create changes in the aquifer's electrical and hydraulic characteristics. Since the electrical responses nearly returned to pre-injection levels during the EOR testing, the volume of water added was almost inconsequential with regards to the overall volume of the aquifer. This indicates that insufficient volume of water was used to result in substantial changes in electrical properties.

4. **Comparison of the two-dimensional contour plots of the changes in the imposed electric field shows effects that appear related to fluid flow. Flow directions, volumetric differences, and structural barriers to flow at the reservoir level can be extracted from the HRR data. All of the electrical responses appear to support the observed production data and offer reasonable explanations for the relatively poor performance of the surfactant test.**

   Well 73S34 reported the highest water production of the four production wells. The combination of higher water production and lower transfer resistance appears to be correlated. This suggests a general flow path to the north. The extent of the low transfer resistance to the north may explain the fluid migration path of water and surfactant injected into well 63S34. The northern fault seems to have a permeable horizon at the equivalent depth as the Shannon, which allows fluid to flow to the north across the fault. On the other hand, the southern fault and the weak low associated with injection well 65SX34 suggest a correlation between it and the southern fault.

   There is a highly pronounced northwest-southeast orientation of changes in the electric field (dashed red line on the residual E-field Figures 20 and 23) that may indicate preferential flow directions. This orientation appears to agree with the known structural trends (i.e. dip) within the electrical mapping area, but no fault has been mapped there. The boundary is interpreted as a change in intrinsic permeability and could be due to either a fault or a facies change. The majority of the low values are to the west of the interpreted barrier for well 65SX34 injections whereas the majority of the low values are to the north for 63S34 injections. The barrier interpreted from 65SX34 and 63S34 datasets, appears to truncate against the north fault and perhaps against the southern fault.

   The sharp gradient (E-field Figure 22) between injection well 65SX34 and 65-56S34 is interpreted to indicate the presence of the southern fault and that the fault exists in close proximity to the injection level for well 65SX34. This interpretation is supported by the much shorter aquifer recovery time determined by the time-series analysis. Figures 20 and 23 show the change in transfer resistance between the start and end of the test as observed relative to injection wells 63S34 & 65SX34 respectively, after all injections. A comparison of the two figures shows that the general magnitude of the low for 65SX34 is much less than that associated with well 63S34. The magnitude differences suggest that

less fluid accumulated in the Shannon reservoir in the area of 65SX34. It is likely that much of the fluid migrated down the southern fault.

5. **Reliability of the HGI Instrument Trailer, the data acquisition system and the remote satellite communication systems were demonstrated by four months of field testing.**
6. **Despite the insignificant change in oil and water in the production wells, the HRR monitoring technology had sufficient sensitivity to enable identification of changes in spatial and temporal fluid flow characteristics, indicating why and where the fluids were moving.**
7. **HRR technology proved to be a cost effective technology easily integrated into new and existing oilfields to provide accurate analysis of EOR methods.**
8. **Deployment of the HRR technology occurred during active oil production with minimal intrusion in the daily oilfield operations.**

7.0 REFERENCES

Barnett, D.B., G.W. Gee, and M.D. Sweeney, 2002, Results of Tank-Leak Detection Demonstration Using Geophysical Techniques at the Hanford Mock Tank Site—Fiscal Year 2001, PNNL-13818, Pacific Northwest National Laboratory, Richland, Washington.

Barnett, D.B., G.W. Gee, M.D. Sweeney, M.D. Johnson, and others, 2003, Results of Performance Evaluation Testing of Electrical Leak-Detection Methods at the Hanford Mock Tank Site—FY 2002, PNNL-14192, Pacific Northwest National Laboratory, Richland, Washington.

Burke, C.A., 2006, Tank 241-S-102 High-Resolution Resistivity Leak Detection and Monitoring Testing Report, RPP-30121, CH2M HILL Hanford Group, Inc., Richland, Washington.

Cooper, H. H., Jr., J. D. Bredehoeft, and I. S. Papadopulos, 1967, Response of a Finite-Diameter Well to an Instantaneous Charge of Water, Water Resources Research, Vol. 3, No. 1, pp. 263-269.

Cooper, S. P., L. B. Goodwin, & J. C. Lorenz, 2006, Fracture and fault patterns associated with basement-cored anticlines: The example of Teapot Dome, Wyoming, AAPG Bulletin, Vol. 90, No. 12, pp. 1903-1920.

Fetter, C. W., 2001, Applied Hydrology, Prentice Hall, New Jersey.

Freeze, R.A. and J.A. Cherry, 1979, Groundwater, Prentice Hall, New Jersey.

Fink, J. B., 2007, U.S. Patent 7,141,982, Estimation of Leakage Rates Using Voltage Measurements.

Goehring, S. and C. L. Davidson, 2001, Evaluation of fractures for future oil production in the Steele Shale: Naval Petroleum Reserve No. 3, Teapot Dome, Wyoming, RMOTC.

Hvorslev, M. J., 1951, Time lag and soil permeability in groundwater observations, U.S. Corps of Engineers, Waterways Experiment Station Bulletin 36, Vicksburg, MS.

Komor, P. D., 1999, Underground Tank Technology Update, Vol. 13, No. 1, Dept. of Engineering Professional Development, Univ. of Wisconsin – Madison.

Papadopulos, I. S., J. D. Bredehoeft, and H. H. Cooper, Jr., 1973, On the analysis of ‘slug test’ data, Water Resources Research, Vol. 9, No. 4, pp. 1087-1089.

Schofield, J.S., 2006, SST Deployment Demonstration and Injection Leak Testing of the HRR Long Electrode LDM System, RPP-17191, CH2M Hill Hanford Group, Inc., Richland, Washington.

8.0 TABLES

Table 1: Water Surfactant Injections

Water-Surfactant Injections

Date	HGI Day	Time	Fluid	bbls	Well	Date	HGI Day	Time	Fluid	bbls	Well
26-Jun	2369	11:00 to 11:20	Water	75		28-Aug	2432	14:15 to 14:47	1.5% Surfactant	70	65-S-34
27-Jun	2370	10:00 to 10:20	Water	70	63-S-34	29-Aug	2433	10:45 to 11:15	1.5% Surfactant	70	65-S-34
28-Jun	2371	8:00 to 8:20	Water	70	63-S-34	30-Aug	2434	15:45 to 16:11	1.5% Surfactant	70	65-S-34
29-Jun	2372	11:30 to 11:50	Water	70	63-S-34	31-Aug	2435	10:45 to 11:21	1.5% Surfactant	70	65-S-34
3-Jul	2376	8:30 to 9:00	Water	70	65-S-34	4-Sep	2439	Labor Day	None	0	63-S-34
4-Jul	2377	8:00 to 8:30	Water	70	65-S-34	5-Sep	2440	1:00 to 1:30	1.5% Surfactant	70	63-S-34
5-Jul	2378	8:30 to 8:50	Water	70	65-S-34	6-Sep	2441	1:00 to 1:30	1.5% Surfactant	70	63-S-34
6-Jul	2379	9:55 to 10:15	Water	70	65-S-34	7-Sep	2442	8:00 to 8:30	1.5% Surfactant	70	63-S-34
10-Jul	2383	11:50 to 12:10	Water	70	63-S-34	11-Sep	2446	8:30 to 9:00	1.5% Surfactant	70	65-S-34
11-Jul	2384	11:32 to 12:10	Water	50	63-S-34	12-Sep	2447	9:45 to 10:15	1.5% Surfactant	70	65-S-34
12-Jul	2385	2:50 to 3:10	Water	70	63-S-34	13-Sep	2448	15:30 to 16:00	1.5% Surfactant	70	65-S-34
13-Jul	2386	9:35 to 10:55	Water	70	63-S-34	14-Sep	2449	8:00 to 8:30	1.5% Surfactant	70	65-S-34
17-Jul	2390	8:30 to 8:50	Water	70	65-S-34	18-Sep	2453	8:30 to 9:00	1.5% Surfactant	70	63-S-34
18-Jul	2391	7:35 to 7:50	Water	70	65-S-34	19-Sep	2454	8:30 to 9:00	1.5% Surfactant	70	63-S-34
19-Jul	2392	8:30 to 9:00	Water	70	65-S-34	20-Sep	2455	9:30 to 10:00	1.5% Surfactant	70	63-S-34
20-Jul	2393	8:20 to 8:40	Water	70	65-S-34	21-Sep	2456	10:30 to 11:00	1.5% Surfactant	70	63-S-34
24-Jul	2397	8:50 to 9:22	1.5% Surfactant	70	63-S-34	25-Sep	2460	9:00 to 10:00	Water	70	65-S-34
25-Jul	2398	8:30 to 9:05	1.5% Surfactant	70	63-S-34	26-Sep	2461	weather	None	0	65-S-34
26-Jul	2399	8:00 to 8:30	1.5% Surfactant	70	63-S-34	27-Sep	2463	13:00 to 13:30	Water	70	65-S-34
27-Jul	2400	8:35 to 10:05	1.5% Surfactant	70	63-S-34	28-Sep	2464	8:30 to 9:00	Water	70	65-S-34
31-Jul	2404	8:15 to 8:43	1.5% Surfactant	70	65-S-34	2-Oct	2468	14:45 to 15:15	Water	70	63-S-34
1-Aug	2405	8:17 to 9:30	1.5% Surfactant	70	65-S-34	3-Oct	2469	8:00 to 8:30	Water	70	63-S-34
2-Aug	2406	15:30 to 16:37	1.5% Surfactant	70	65-S-34	4-Oct	2470	13:00 to 13:30	Water	70	63-S-34
3-Aug	2407	13:15 to 15:50	1.5% Surfactant	70	65-S-34	5-Oct	2471	weather	None	0	63-S-34
7-Aug	2411	08:00 to 11:50	1.5% Surfactant	70	63-S-34	9-Oct	2475	weather	None	0	65-S-34
8-Aug	2412	11:58 to 12:15	1.5% Surfactant	70	63-S-34	10-Oct	2476	weather	None	0	65-S-34
9-Aug	2413	08:35 to 09:00	1.5% Surfactant	70	63-S-34	11-Oct	2477	8:00 to 8:30	Water	70	65-S-34
10-Aug	2414	08:25 to 08:50	1.5% Surfactant	70	63-S-34	12-Oct	2478	14:30 to 15:00	Water	70	65-S-34
14-Aug	2418	09:30 to 10.26	1.5% Surfactant	70	65-S-34	16-Oct	2481	16:00 to 16:30	Water	70	63-S-34
15-Aug	2419	08:15 to 08:45	1.5% Surfactant	70	65-S-34	17-Oct	2482	8:15 to 9:45	Water	70	63-S-34
16-Aug	2420	08:15 to 08:45	1.5% Surfactant	70	65-S-34	18-Oct	2483	16:19 to 16:48	Water	70	63-S-34
17-Aug	2421	08:25 to 08:50	1.5% Surfactant	70	65-S-34	19-Oct	2484	11:00 to 11:23	Water	70	63-S-34
21-Aug	2425	12:50 to 01:10	1.5% Surfactant	70	63-S-34	23-Oct	2488	8:18 to 8:48	Water	70	65-S-34
22-Aug	2426	03:25 to 03:35	1.5% Surfactant	70	63-S-34	24-Oct	2489	13:37 to 14:06	Water	70	65-S-34
23-Aug	2427	09:00 to 09:30	1.5% Surfactant	70	63-S-34	25-Oct	2490	8:34 to 8:58	Water	70	65-S-34
24-Aug	2428	10:00 to 10:20	1.5% Surfactant	70	63-S-34	26-Oct	2491	weather	None	0	65-S-34

Madison Formation Water
Water only Injection = 2,155 bbls

1.5 % Surfactant
2,415 bbls Madison Formation Water mixed with 35 bbls Surfactant: Total Injection = 2,450 bbls

Table 2: Production Wells

Production Wells

Date	54/55-S-34		73-S-34		84-S-34			54/55-S-34		73-S-34		84-S-34	
	oil, bpd	water, bpd	oil, bpd	water, bpd	oil, bpd	water, bpd		oil, bpd	water, bpd	oil, bpd	water, bpd	oil, bpd	water, bpd
12-Jul							4-Sep						
13-Jul							5-Sep			0.9	2.3	0.9	0.8
14-Jul	0.7	2.3					6-Sep	0.9	1.5	1.1	3.0	1.0	1.0
15-Jul	0.6	1.9					7-Sep			0.7	3.1	0.7	1.3
16-Jul	0.6	1.8					8-Sep	0.0	1.4				
17-Jul	0.6	1.8	1.4	3.7			9-Sep	1.0	1.7				
18-Jul	0.8	2.0	2.7	11.9	0.7	1.2	10-Sep	1.1	1.6				
19-Jul	0.8	2.0	0.7	5.2	0.6	1.3	11-Sep	1.0	1.4				
20-Jul			0.6	4.5	0.4	1.5	12-Sep	0.9	1.7	0.4	3.3	0.3	1.6
21-Jul	0.9	2.0	0.4	4.4	0.6	1.3	13-Sep	1.0	1.5	0.5	3.3	0.4	1.6
22-Jul	0.7	1.6	0.4	4.4	0.6	1.3	14-Sep	1.1	1.7	0.5	3.6	0.4	1.7
23-Jul	1.0	1.5					15-Sep			0.4	3.6	0.5	1.5
24-Jul	1.0	1.7					16-Sep			0.2	3.4	0.4	1.4
25-Jul	0.9	1.6	0.5	3.7	0.5	1.3	17-Sep			0.3	3.0	0.3	1.2
26-Jul	1.0	1.7	0.6	4.0	0.6	1.4	18-Sep	0.9	1.7				
27-Jul	0.9	1.6	0.5	3.7	0.4	1.5	19-Sep	1.0	1.5				
28-Jul	1.1	1.7					20-Sep	1.2	1.5	0.8	3.1	0.7	1.2
29-Jul	1.0	1.1					21-Sep			0.7	4.7	1.2	1.9
30-Jul	1.1	1.6					22-Sep	1.8	3.6				
31-Jul	0.9	1.7					23-Sep	0.9	1.6				
1-Aug	1.0	1.7	0.7	3.2	0.6	1.2	24-Sep	0.9	1.6				
2-Aug	1.0	1.7	0.6	3.4	0.4	1.5	25-Sep	0.9	1.6	0.8	3.1	0.8	1.0
3-Aug	1.0	1.6	0.6	3.5	0.6	1.5	26-Sep	1.1	1.5	0.7	3.0	0.7	1.2
4-Aug	1.0	1.7					27-Sep	1.1	1.4	0.7	3.1	0.6	1.0
5-Aug							28-Sep	0.9	1.6				
6-Aug	1.0	1.6					29-Sep	1.2	1.7				
7-Aug	0.9	1.5					30-Sep	1.1	1.6				
8-Aug	1.1	1.6	0.6	3.5	0.7	1.4	1-Oct	1.0	1.5				
9-Aug	1.0	1.6	0.5	3.7	0.7	1.2	2-Oct	1.1	1.5				
10-Aug	1.0	1.6					3-Oct	1.0	1.7				
11-Aug	1.0	1.7					4-Oct	0.9	1.6	0.7	3.2	0.8	1.7
12-Aug	1.0	1.6					5-Oct	1.0	1.6	0.9	2.9	1.0	0.7
13-Aug	0.9	1.9					6-Oct	1.1	1.7				
14-Aug	0.9	1.3					7-Oct	1	1.5				
15-Aug	1.0	1.7	0.4	3.6	0.5	1.5	8-Oct	1	1.6				
16-Aug	1.0	1.6	0.2	3.4	0.4	1.4	9-Oct	0.9	1.7				
17-Aug	1.0	1.6	0.3	3.0	0.3	1.2	10-Oct	0.7	1.7	0.9	2.5	0.7	1.6
18-Aug	0.9	1.7					11-Oct	1.0	1.9	0.9	2.5	1.0	1.4
19-Aug	1.0	1.5					12-Oct	0.8	1.7	0.7	2.8	0.8	1.2
20-Aug	1.1	1.7					13-Oct						
21-Aug	1.0	1.6					14-Oct						
22-Aug	1.0	1.5					15-Oct						
23-Aug	1.0	1.5					16-Oct	0.9	1.6				
24-Aug	1.1	1.7					17-Oct	0.9	1.8	1.0	1.2	0.7	0.7
25-Aug	0.9	1.5					18-Oct	0.7	1.7	1.2	2.0	0.9	0.9
26-Aug	0.9	1.7					19-Oct	0.9	1.6				
27-Aug	0.9	1.6					20-Oct	1.3	1.6	0.8	2.6	1.0	1.0
28-Aug	0.9	1.7					21-Oct	0.8	1.7				
29-Aug	0.9	1.6	0.3	3.5	0.6	1.2	22-Oct	0.9	1.4				
30-Aug	1.2	1.7	0.6	3.4	0.6	1.4	23-Oct	1.1	1.6				
31-Aug	1.0	1.7	0.3	3.5	0.4	1.4	24-Oct	1.1	1.6	1.0	2.1	0.8	0.7
1-Sep	0.9	1.4					25-Oct	1.3	1.5	1.0	1.9	0.9	0.8
2-Sep	0.8	1.8					26-Oct			1.0	2.0	0.9	1.0
3-Sep	1.3	1.3											
						Average		**0.9**	**1.6**	**0.7**	**3.5**	**0.6**	**1.3**

Table 3: Water Analysis of Selected Test Wells

Location	pH	Silica as Major Ion	Silica as Metal
		mg/l	mg/l
1.5% Surfactant Solution		254,000	119,000
Madison Water, 57-WX-3		65.1	30.4
Shannon Base		12.0	5.6
63-S-34		74.7	34.9
65-SX-34		91.3	42.7
43-A-34	7.54	6.9	3.2
54-S-34 (Production)	7.65	11.5	5.4
55-S-34 (Production)	6.86	8.6	4.0
73-S-34 (Production)	7.02	11.8	5.5
84-S-34 (Production)	6.95	10.7	5.0